Lawrence Berkeley National Laboratory
LBL Publications

Title

A g-Ray Tracking Algorithm for the GRETA Spectrometer

Permalink

https://escholarship.org/uc/item/0pw1f27w

Authors

Schmid, G J
Deleplanque, M A
Lee, I Y
et al.

Publication Date

1999-02-01

eScholarship.org Powered by the California Digital Library
University of California

LBNL-42912
Preprint

ERNEST ORLANDO LAWRENCE
BERKELEY NATIONAL LABORATORY

A γ-Ray Tracking Algorithm for the GRETA Spectrometer

G.J. Schmid, M.A. Deleplanque, I.Y. Lee,
F.S. Stephens, K. Vetter, R.M. Clark,
R.M. Diamond, P. Fallon, A.O. Macchiavelli,
and R.W. MacLeod

Nuclear Science Division

February 1999

Submitted to
Nuclear Instruments and Methods in Physics Research Part A

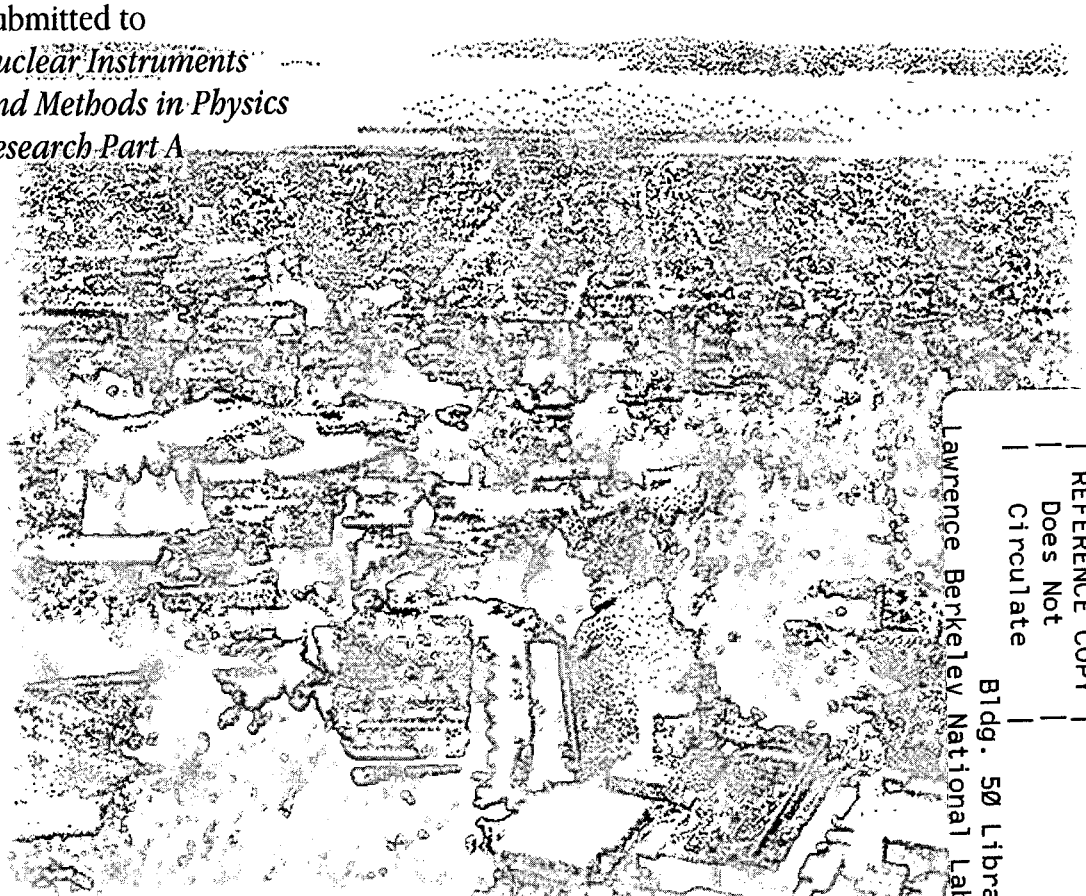

REFERENCE COPY
Does Not
Circulate

Bldg. 50 Library - Ref.
Lawrence Berkeley National Laboratory

Copy 1

LBNL-42912

DISCLAIMER

This document was prepared as an account of work sponsored by the United States Government. While this document is believed to contain correct information, neither the United States Government nor any agency thereof, nor the Regents of the University of California, nor any of their employees, makes any warranty, express or implied, or assumes any legal responsibility for the accuracy, completeness, or usefulness of any information, apparatus, product, or process disclosed, or represents that its use would not infringe privately owned rights. Reference herein to any specific commercial product, process, or service by its trade name, trademark, manufacturer, or otherwise, does not necessarily constitute or imply its endorsement, recommendation, or favoring by the United States Government or any agency thereof, or the Regents of the University of California. The views and opinions of authors expressed herein do not necessarily state or reflect those of the United States Government or any agency thereof or the Regents of the University of California.

LBNL-42912

A γ-Ray Tracking Algorithm for the GRETA Spectrometer

G.J. Schmid, M.A. Deleplanque, I.Y. Lee, F.S. Stephens, K. Vetter, R.M. Clark, R.M. Diamond, P. Fallon, A.O. Macchiavelli, and R.W. MacLeod

Nuclear Science Division
Ernest Orlando Lawrence Berkeley National Laboratory
University of California
Berkeley, California 94720

February 1999

This work was supported by the Director, Office of High Energy Nuclear Physics, Nuclear Physics Division, of the U.S. Department of Energy under Contract No. DE-AC03-76SF00098.

A γ-Ray Tracking Algorithm for the GRETA Spectrometer

G.J. Schmid, M.A. Deleplanque, I.Y. Lee, F.S. Stephens, K. Vetter, R.M. Clark,

R.M. Diamond, P. Fallon, A.O. Macchiavelli, R.W. MacLeod

Lawrence Berkeley National Laboratory, University of California, Berkeley, CA 94720

Abstract: We discuss a γ-ray tracking algorithm that has been developed for the proposed Gamma Ray Energy Tracking Array (GRETA). This algorithm has been designed so as to maximize the resolving power for detecting high-multiplicity γ-ray events. The conceptual basis for this algorithm will be presented. In addition, Monte Carlo simulated data will be used to assess performance over a large range of relevant parameters. A discussion of the potential γ-ray polarimeter performance of GRETA is also presented.

1. Introduction

A new 4π γ-ray detector array is currently being developed by the nuclear structure group at the Lawrence Berkeley National Laboratory (LBNL). This array, known as the Gamma-Ray Energy Tracking Array (GRETA), will use the technique of γ ray tracking to improve detection of high multiplicity γ-ray cascades. The resolving power of GRETA should exceed that of existing arrays [1,2] by more than two orders of magnitude.

The concept behind GRETA has been discussed in recent papers [3,4]. The fundamental idea is to replace the modules of Compton suppressed Ge detectors that comprise the current arrays with a spherical shell of ~100 highly segmented Ge detectors. Rather than suppress those γ rays that escape from one detector into another, the goal of the GRETA array is instead to track each γ ray throughout its path and attempt to recover its full energy.

Research and development into GRETA has focused on two areas. The first has been the experimental study of charge/current pulse shapes in a single GRETA prototype detector [4]. The goal here has been to benchmark techniques for determining the position and energy of γ-ray interactions in a highly segmented, co-axial Ge detector. The second area of research has been to benchmark a γ ray tracking algorithm for resolving the tracks of multiple, coincident, γ rays, and that is the subject of this paper. In the discussion that follows, the focus will be on describing the algorithm that has been developed, and also presenting its results as a function of several important parameters. These parameters will include: γ ray energy, E_γ; γ ray multiplicity, M (which is the number of coincident γ-rays incident on the array); and also the attainable position resolution in the array, Δr.

2. Definition of problem

2.1 GRETA geometry

Preliminary designs for GRETA are based on a shell with an inner radius of 12cm and an outer radius of 21 cm. These dimensions are arrived at by considering the size of

currently available co-axial Ge detectors, the need for space between target and detector to accommodate auxiliary detectors, and the cost of the array. For nuclear structure studies, the beam would enter through a hole on one side, interact with the target at the center, and exit through a hole on the other side. In what follows, an algorithm will be developed and tested using a simple spherical shell of Ge with r_1=12cm and r_2=21 cm. Results for a more realistic geometry, consisting of 120 close packed, tapered, high purity Ge detectors (including Al housing cans), will be presented at the end.

2.2 Scenarios considered

The γ-ray tracking algorithm was developed with some likely scenarios in mind. In particular, the search for, and description of, superdeformed and hyperdeformed bands. Experimental studies in this regime are characterized by high-fold data analysis. For example, the formation and decay of a superdeformed band typically involves the emission of 3-5 neutrons, with E_n=1-5 MeV, and 20-25 γ rays, with E_γ=0.1-2.0 MeV. These particles will hit the Ge shell nearly simultaneously (with a small time delay between γ rays and neutrons), and thus a considerable number of interaction points can be expected. For example, 25 coincident 1.3 MeV γ rays would be expected to give ~100 γ-ray interaction points in the Ge shell (neglecting electron tracks). The accompanying neutrons will add more interaction points, but we would seek to eliminate these by using stringent time cuts.

2.3 Monte Carlo simulation

The performance of the γ-ray tracking algorithm was assessed using Monte Carlo simulated events. For the most part, these simulations used the GEANT [5] Monte Carlo code. For simulations involving the simple Ge shell, electron tracks were not included. The reasoning here was that for the energy range of interest, the e- tracks (as initiated by Compton-recoil and photo electrons) are always less than the best attainable position resolutions (~1-2 mm). However, for the realistic GRETA geometry discussed at the end,

electron tracking was included to gauge absorption effects. In situations involving transport of polarized γ rays, the Monte Carlo code of [6] was used.

2.4 Position resolution

The interaction points generated by the Monte Carlo simulation were further processed so as to simulate a position resolution effect in the Ge shell. For cases where the electron tracks were not included, position resolution was effected by simply dividing 3-D space into cubic voxels of side Δr. All interaction points within a given cubic voxel were then added together. For cases where the electron tracks were included, a different scheme, based on clustering of interaction points, was used. This scheme for effecting position resolution is independent of the fixed coordinate system, and thus better handles the real-life complication of electron tracks. In tests that were done, the two schemes gave similar results for the "no electron track" case.

In contrast to the position resolution, the energy resolution is not a sensitive parameter to the overall performance of the algorithm in the GRETA array. This aspect is addressed further in section 3.

2.5 Testing the algorithm

The algorithm was tested using a 32 bit, 75 MHz, SUN sparcstation. Performance was gauged by calculating the GRETA efficiency (ε) and peak-to-total (P/T) values for various scenarios. For each case, the algorithm running time was also noted.

3. The γ-ray tracking algorithm

For a Ge shell (r_1=12cm, r_2=21cm) operated as a single (unsegmented) detector, one would expect excellent performance for single γ-ray events. In particular, Monte Carlo simulation shows that at E_γ=1.332 MeV, the efficiency is 0.7 and the peak-to-total is 0.78.

However, for cases where two or more γ rays hit simultaneously, this mode of operation fails completely (due to summing).

In this section we discuss the details of a γ-ray tracking algorithm that has been developed to handle the case of multiple, coincident, γ rays. The basic function of the algorithm is to process the γ-ray interaction points in the shell so as to determine the number and energy of all incident γ rays. The technique is as follows: organize the interaction points into clusters; evaluate the clusters using Compton tracking; and then sort each cluster into one of several possible groups depending on what operation needs to be done on that cluster in order to recover the complete track of an incident γ-ray.

3.1 Clustering

Because of the forward peaking of the Compton scattering cross section, as well as the decreasing mean free path with decreasing energy, the γ-ray interaction points will tend to be clustered in a 2-dimensional θ-ϕ space (polar coordinates). Because of this, the criteria for clustering the points was set as follows: any two interaction points within a given angle separation (α), as viewed from the origin, are grouped into the same cluster. The angle α is a variable parameter in this scheme, and different values of α will produce different sets of clusters (e.g. for larger α, the number of clusters formed will decrease).

The clustering algorithm works by first assigning polar coordinates θ, ϕ to each interaction point. The interaction points are then ordered by their θ value. For a given point (θ_0, ϕ_0), all non-committed points which have their θ value in the range θ_0 +/- α degrees are searched to see if their ϕ value is consistent with a total angular separation of α degrees, or less, as viewed from the origin. In general, this means that $\Delta\phi$ (=abs[$\phi-\phi_0$]) must satisfy the following relation:

$$\Delta\phi \le \mathrm{abs}\left(\cos^{-1}\left[\frac{\cos\alpha - \cos\theta\cos\theta_0}{\sin\theta\sin\theta_0} \right] \right). \qquad (1)$$

If a point with the desired angular separation is found, it is added to the (θ_0, ϕ_0) cluster. When the initial search using (θ_0, ϕ_0) is complete, subsequent searches are then performed using each of the new points added. This process continues until no new links are found (i.e. the cluster is completely formed). At this stage, we then look at the next non-committed point in the ordered θ queue, and begin forming another cluster. The resulting set of clusters is unique, and depends only on the initial α value which is chosen.

Of the clusters that have been formed, some will exactly correspond to the interaction points of fully-absorbed γ-rays (the "good" clusters) and others will not (the "bad" clusters). For example, bad clusters can arise when two good clusters are misidentified as one, or one good cluster is misidentified as two. Further processing of the bad clusters can be done in order to recover more good clusters (e.g. the bad clusters can be split, added, etc.). However, since this first step of the algorithm is relatively fast, it is worthwhile to evaluate the total performance at this stage (e.g. what are the results if we assume that all clusters created are good clusters).

Figure 1 shows the efficiency and peak-to-total for the clustering-only scenario as a function of α and also as a function of the position resolution of the array. This Figure is for the case of 25 coincident (isotropic) 1.332 MeV γ-rays.[1] The dashed line in Figure 1 shows the measured performance of the Gammasphere array [1], one of the world's most powerful γ-ray spectrometers for nuclear structure studies. It is seen that the current results offer large gains in efficiency but at the cost of peak-to-total. At lower energies, where the γ-ray clusters are more confined, the clustering-only scenario works much better. This is shown in Figure 2, where we have plotted the results for 0.1 MeV.

---

[1] This particular energy was chosen because it corresponds to the well-known ^{60}Co calibration line. The data points in Figure 1, and in most other figures here, represent 10^4 γ-rays launched. In this case, that means 400 M=25 events (which makes the error on each point less than the size of the plotted symbol).

3.2 Compton tracking

In order to determine which original clusters are good, and which need further processing, we want to evaluate the clusters and assign each one a "figure-of-merit". Akin to the approach in [7], we do the evaluation using the energy-angle relationship of the Compton scattering process:

$$E'_\gamma = \frac{0.511}{1+\frac{0.511}{E_\gamma}-\cos\theta_c}, \qquad (2)$$

where E'_γ is the scattered γ-ray energy in MeV, E_γ is the incident γ-ray energy in MeV, and θ_c is the polar scattering angle.

The technique is to assume that the cluster is good (i.e. a full absorption), and that all the N interaction points in it are Compton interactions, except for one, which is a photoabsorption. For a given 3-point combination, we use (2) to construct a figure-of-merit (FM) function which compares the calculated scattering angle, θ_c (based on the energies of the interaction points), to a measured scattering angle, θ_m (based on the positions of the interaction points). By treating the origin as the "zeroth" point, we then look for a one-two combination among the interaction points which minimizes the FM. Having found this 0-1-2 combination, we then use a similar FM minimizing procedure to find the unknown 3rd point in the 1-2-3 scatter. This approach continues until we reach the last 3-point combination, (N–2)-(N–1)-(N). The total FM for the whole cluster is then the sum of these optimum, single scatter, FM's. The lower the total FM, the more likely that the cluster is "good". The 3-point approach that is used here to obtain the total FM requires that we make $N(N-1)+\sum_{n=1}^{N-2} n$ separate calculations.[2]

---

[2] This is small compared to the N! combinations in a rigorous N-point tracking approach. Investigations have concluded that the somewhat larger success rate of the rigorous approach does not merit the greatly increased computing time.

We can formulate our FM calculation in mathematical terms as follows. We start by defining a randomly ordered set of points, P_n, which consists of the n^{th} assumed Compton scatter point as well as all the other cluster points which are assumed to follow it in time. We can then define $E_{j,n}$ ($E_{k,n}$) to be the energy of the j^{th} (k^{th}) point from set P_n. From (2), the n^{th} Compton scatter angle from point j, $\theta_{c\,j,n}$, can then be given as:

$$\theta_{c\,j,n} = \cos^{-1}\left(1.0 + \frac{0.511}{\sum_k E_{k,n}} - \frac{0.511}{\sum_k E_{k,n} - E_{j,n}}\right). \tag{3}$$

For a given three point combination, we can also measure the n^{th} Compton scatter angle from the middle point, j, as follows:

$$\theta_{m\,j,k,n} = \cos^{-1}(\hat{v}_j \cdot \hat{v}_k), \tag{4}$$

where $\hat{v}_j$ is the vector from the $(n\text{-}1)^{th}$ Compton scatter point to the j^{th} point of P_n, and $\hat{v}_k$ being the vector from the j^{th} point of P_n to the k^{th} point of P_n. For n=1, the zeroth Compton scatter point is defined to be the origin.

In this manner, we can define a FM for the n^{th} Compton scatter angle, FM_n, as:

$$FM_{n,j,k} = \left|\frac{\theta_{m\,j,k,n} - \theta_{c\,j,n}}{\Delta\theta_{j,k,n}}\right|, \tag{5}$$

where the denominator is the calculated error on the quantity in the numerator (and is based on the position and energy uncertainties).

To determine the 1st Compton interaction, n=1, we want to minimize (5) with respect to (j,k) by trying all possible 2-point combinations in P_n. For the (n=1) case, the set P_n consists of all N interaction points. To determine subsequent scatters, n>1, we now assume that all previous points <n are known, and thus we only need minimize (5) with respect to k. For these n>1 minimizations, the set P_n consists of all N points *except* those <n. For all cases, the result of the minimization for Compton scatter n is:

$$FM_n = \left|\frac{\theta_{m\,n} - \theta_{c\,n}}{\Delta\theta_n}\right|. \tag{6}$$

After minimizing (5) with respect to all points $n \leq (N-1)$, we can sum up the resulting FM's, (6), and obtain a total FM which is related to the likelihood that the whole cluster is good:

$$FM = \left(\frac{1}{N-1}\right)\sum_{n} FM_n = \left(\frac{1}{N-1}\right)\sum_{n=1}^{N-1}\left|\frac{\theta_{m\,n} - \theta_{c\,n}}{\Delta\theta_n}\right|. \qquad (7)$$

This FM is not defined for those clusters that have only one point. The one-point clusters are assumed to be Compton escape events, and are thrown out (note: this differs from the clustering-only scenario, where single hit events are kept). Throwing out single hit events will lead to decreased efficiency at the lower energies, but improved peak-to-total at the higher energies.

It should be noted that for the Ge detector array under consideration, the total error, $\Delta\theta_n$, is always dominated by errors in $\Delta\theta_{m\,n}$ (i.e. by the position resolution). This can be seen by realizing the following:

$$\frac{\Delta\theta_{m\,n}}{\theta_{m\,n}} \sim \frac{\Delta r}{\lambda}, \quad \text{while} \quad \frac{\Delta\theta_{c\,n}}{\theta_{c\,n}} \sim \frac{\Delta E_\gamma}{E_\gamma}, \qquad (8)$$

where Δr is the position resolution, λ is the mean free path for the Compton interaction, and ΔE_γ is the energy resolution. Since we eventually expect $\Delta r \sim 1$mm, $\lambda \sim 1$cm, and $\Delta E_\gamma \sim 2$ keV (for a 1.3 MeV γ-ray scattering in Ge), we see that $\frac{\Delta\theta_{m\,n}}{\theta_{m\,n}} \sim 0.1$ and $\frac{\Delta\theta_{c\,n}}{\theta_{c\,n}} \sim 0.01$.

3.3 Further processing of clusters: the cluster modes

As we showed in Figure 1, only about 30% of the originally defined clusters will correspond to actual incident γ-rays for an M=25, E_γ=1.332 MeV event. The other clusters will need further processing. For example, Figure 3 shows the "cluster modes" that are present when 25 1.332 MeV γ-rays hit the Ge shell. A given mode describes the operation that must be done on a formed cluster in order to recover an actual incident γ-ray.

Here are some of the modes that have been identified:

a). Original mode - Cluster is good "as-is" (i.e. it matches an incident γ-ray).

b). Add mode - Cluster can be added to another cluster in order to recover

an incident γ-ray.

c). Split mode - Cluster can be split such that one of the resulting subclusters then forms a good incident γ-ray.

d). Split-Add mode - Cluster can be split such that one of the resulting subclusters can be added to another cluster in order to recover an incident γ-ray.

In Figure 3, the relative probability of some of these modes are plotted as a function of the angle parameter α.

In order to identify the mode of each cluster, we can use the tracking-based figures-of-merit introduced in section 3.2. For example, the "original" cluster FM will help identify mode a. In order to address mode b, clusters can be added together to form superclusters. These superclusters are then tracked using the same technique described in the section 3.2. The resulting figure-of-merit is called the "add" FM. In order to address mode c, each cluster can be split in a prescribed manner into two subclusters. These subclusters can then be individually tracked using the techniques of the section 3.2. The resulting FM's are called the "split" FM's. Finally, in order to address mode d, we can take the subclusters created in the split mode analysis, and look to add them to original clusters in order to form good clusters. These split-add clusters can be tracked in order to form "split-add" FM's.

The cluster splitting procedure is complex enough to require further explanation. In order to split a cluster, we first construct a "moment-of-inertia" matrix using the positions of the cluster interaction points (where each point is assigned a unit "mass"). By diagonalizing this matrix, we are able to identify the three principal axes. The interaction points are then projected onto these three axes, and we look for the largest two gaps on each axis. These gaps, six in total, form candidate split points for the cluster. In separate analyses, the cluster is then split using each of the candidate split points, and the resulting sub-clusters are tracked. This yields a total of 12 FM's for each cluster. The lowest FM is

then assigned as the "split" FM for the cluster, representing the probability that a split operation is actually the correct operation for this cluster. The sub-cluster with the best FM will have a partner sub-cluster. This partner sub-cluster can be added to other original clusters, and the resulting split-add cluster can be tracked. This forms the "split-add" FM.

3.4 Cluster sorting

One technique for cluster sorting [3] is to calculate all possible FM's for each cluster (e.g. original, add, split, etc.), and then perform a splitting in the multi-dimensional FM space so as to determine the proper mode for the cluster. However, this procedure has proved too computationally time consuming. Therefore, a stepwise approach with regard to the FM calculations has been undertaken. In particular, the FM's are calculated in order. Only those clusters which fail a one-dimensional FM cut in one step (i.e. where the FM is above the cutoff) are propagated to the next step. Those clusters which survive a given cut are selected to be of that mode. In this manner, the time consuming add and split-add operations are only performed on a small subset of the entire cluster set. Figure 4a shows a histogram of the "original" figure-of-merit (OFM) for a position resolution of 1mm. The solid line shows the good clusters, while the dashed line shows all the other cluster types. Figure 4b shows the "add" figure-of-merit (AFM) for those clusters that failed an OFM<80 cut in 4a. These two figures show that good clusters can be selectively identified using the OFM, while the add clusters can be selectively separated out from the remaining clusters using the AFM.

In order to obtain the optimal cuts for each mode, the algorithm was tested using Monte Carlo data. By calculating ε and P/T for many possible combinations of cuts (i.e. using a grid search in the cut space), an optimum set of cuts was derived for given energy and multiplicity scenarios. We will refer to these as the "locally-optimized" set of cuts. However, a real-life situation will have energy and multiplicity distributions which are initially unknown. For this reason, it is also useful to have a single set of cuts which will

operate well over a large range of possible energy and multiplicity distributions. This single set of cuts will be referred to as the "globally-optimized" set of cuts.

The procedure used to produce the sets of optimized cuts necessitated the formulation of an explicit "trade-off" function which relates the overall performance to ε and P/T. In order to produce the current set of optimized cuts, a trade-off function known as the resolving power (RP) was used. Under a given set of assumptions, the resolving power for GRETA, as a function of ε, P/T, is derived in [4].

3.5 Cuts on macroscopic quantities

A small improvement in algorithm performance is gained by requiring that acceptable clusters give macroscopic quantities within a prescribed range. Some macroscopic quantities that have been considered are: energy and position moments; number of interaction points; angular separation between clusters (for adding purposes). By performing a grid search among these parameters, and maximizing the resolving power, ideal cuts can be arrived at for given energy and multiplicity scenarios. As with the figure-of-merit cuts, the macroscopic quantity cuts can be locally/globally optimized.

4. Algorithm results for Ge shell

4.1 Recovery of different modes

Figure 5 shows the possible cluster modes and their recovery using the current algorithm for M=25, E=1.332 MeV (locally optimized). The tradeoff in the add and split modes, versus angle parameter, yields an optimum performance at 10°.

4.2 Results versus energy, position resolution, and angle parameter

Figure 6 shows the ε and P/T results for the current algorithm at M=25 and E=1.332 MeV. The performance is gauged as a function of the clustering angle parameter (α) and position resolution. The dashed line represents the measured performance of

Gammasphere. Figure 7 shows the performance of the current algorithm as a function of energy and position resolution (for α=10°). Figure 8 gauges the performance of the algorithm as a function of M and α at a position resolution of 1mm. In this figure, the results fall off sharply as one approaches M=25. This is to be expected due to the increased overlap of γ-ray clusters.

4.3 Computer processing time

Figure 9 shows the average event processing time for the current algorithm in milli-seconds as a function of position resolution. As the position resolution worsens, the number of interaction points decreases (due to individual interaction points being added together),and this causes the computing time to decrease. Figure 10 shows the average event processing time as a function of M, while Figure 11 shows the average event processing time versus α and E_γ. There is a general trend to increase computing time as one increases α, and this is simply due to the increased number of points per cluster (increasing the number of points per cluster is more time consuming than increasing the number of clusters). The trend towards longer computing time at higher energies is also due to more interaction points. Figure 12 shows the average event processing time for each component subroutine as a function of α.

Figures 9-12 have given the event processing time based on a 75 MHz SUN sparcstation. Current state-of-the-art is already more than a factor of 4 faster. If one extrapolates 5 years into the future using the rule-of-thumb "power law" for computer speed (i.e. state-of-the-art computer speed increases about a factor of 2 each year), another factor of 32 is realized. It is thus possible that a 100 fold increase in computing speed could be attained by the time GRETA is built.[3]

---

[3] In fact, the GRETA discussion in [4] makes this assumption, and thus quotes the processing time for M=25, E_γ=1.3 MeV, as "~1ms per event" (instead of the ~100ms/event shown here). Based on this, a final GRETA array with 10^3 parallel processing computers would run at ~1μs/event.

4.4 Local optimization vs. global optimization

As referred to in section 3, figure-of-merit cuts can be determined in a locally or globally optimized fashion. Although the locally-optimized operation produces better performance in all cases, the globally-optimized approach is much simpler to implement, much more practical in real-world situations, and can give results which are not much worse. Figure 13 shows ε and P/T for both cases in a given scenario.

4.5 Application of algorithm to simulated spectra.

Real-world applications of the GRETA array will not involve mono-energetic γ-rays, but instead will focus on arbitrary energy distributions. Figure 14 shows the ε and P/T that result when exposing the GRETA array to the γ-rays from the decay of superdeformed band-1 in ^{152}Dy. This was the first superdeformed band discovered using γ-ray spectroscopy [8], and involves 21 coincident γ-rays in the energy range E=0.6-1.5 MeV. Shown in Figure 14 are the results from the globally-optimized performance (solid line) and the locally-optimized performance (dashed line). The locally-optimized results are obtained using cuts optimized for E=1.0 MeV. It can be seen that the two cases give fairly similar results.

4.6. Neutron background

Neutron background is a potential problem for γ ray tracking techniques. At the energies of interest, ~1 MeV, neutrons interact with Ge primarily by elastic scattering. Using energy and momentum conservation, one can show that a maximum of ~5% of the neutron energy can be lost in each scatter. With a mean free path of about 4cm, a 1 MeV neutron will scatter ~5-6 times and then leave the Ge shell without absorbing.

To avoid intermingling of the γ-ray and neutron interaction points, time cuts must be used. In particular, since neutrons travel slower than γ rays, one can seek to eliminate them by discarding all interactions occurring after some fixed time following the accelerator

beam burst. Tests have shown that a ~15ns time cut, if possible, would serve quite well. The majority of neutron interaction points are eliminated, and those that remain are tightly clustered, and promptly eliminated during the γ-ray tracking phase of the algorithm (these small neutron clusters mimic bad γ-ray clusters, and thus have bad figures-of-merit).

Another potential problem is the less frequent case of inelastic neutron scattering. This type of event will produce γ rays that correspond to the first few excited states in the Ge isotopes. Further study on this aspect of neutron background is recommended.

5. Gamma-ray polarization sensitivity

The projected high position resolution of GRETA leads to the possibility that, in addition to use as a spectrometer, the array could find use as a powerful Compton polarimeter. Typical γ-ray Compton polarimeters [9,10] operate by measuring an azimuthal asymmetry in the Compton scattering (an up-down/left-right scattering asymmetry), and relating this to the incident γ-ray polarization. The more accurately one can measure the azimuthal scattering angle, the more accurate the polarimeter.

The first step in operating GRETA as a polarimeter is to identify the first two interaction points in the Compton scattering of a γ-ray. This information is determined in the tracking stage of the algorithm. Figure 15 shows, for two different energies (at M=1), the fraction of γ-rays which have had their 1st and 2nd points correctly identified by the algorithm. The results are shown as a function of position resolution. At 1mm, the results show a 95% and 90% success rates for E_γ=1.4 MeV and 0.4 MeV respectively. The better performance at E_γ=1.4 MeV is due to the better angular resolution afforded by the larger mean free path at this energy.

Given that the identification success rate is quite high for the 1st two interaction points, it is interesting to see what the actual polarization sensitivity of the GRETA detector is as a function of position resolution and energy. The polarization sensitivity, Q, is simply the proportionality constant which relates the measured experimental asymmetry, A, to the

incident γ-ray polarization, P. Figure 16 shows the measured Q as a function of Δr for E=0.4 MeV. At infinitesimal resolution (Δr=0), one recovers the maximum Q allowed by the Klein-Nishina formula (which gives the polarization sensitivity of the Compton scattering process). As the resolution worsens, Q approaches 40%. These projected GRETA results are compared to the measured results of the Gammasphere segmented Ge detectors [6]. Figure 17 shows the Q as a function of E_γ.

6. Realistic GRETA geometry

Until now, results have been presented only for the simplified geometry of a Ge shell of inner radius 12cm and outer radius 21cm. To gauge the performance of the algorithm on a more realistic geometry, we have designed a GEANT Monte Carlo simulation which incorporates a close-packed 120 detector configuration. The first 110 of these detectors are hexagonal, tapered, co-axial Ge detectors. This preliminary packing leaves 12 pentagonal holes. Ten of these holes are filled with pentagonal, tapered, co-axial Ge detectors. Two pentagonal holes are left for entrance and exit of the incident beam. Each Ge detector (Ge crystal + Al housing can) has a gap of 0.5mm on all sides (i.e. the close-packed detectors are not actually touching).

The hexagonal detectors are positioned so that their front faces are exactly 12cm from the origin (target), while the pentagonal detectors are 12.09cm back. The length of the detectors is set at 9cm, and the taper of each detector is 10°. Each detector consists of a Ge crystal (hole diameter of 8mm) and a surrounding Al housing structure which is 0.5 mm in thickness, and is offset from the Ge crystal by a gap of 1mm.

Figure 18 shows, by the diamond data points, the results (at M=25, E=1.332 MeV) for the realistic GRETA geometry including electron tracking. A conservative position resolution of 2mm is assumed. One observes a substantial drop in performance as compared with the simple Ge shell results presented earlier (shown here as solid circles). The two curves for the realistic geometry (with and without electron tracking), show the

relative contribution of two factors which decrease performance: loss of solid angle to the inter- and intra- detector gaps; and also, loss of full energy events due to electron absorption in Al. For the case of the efficiency, the largest drop is due to the loss in solid angle. For the peak-to-total, the electron absorption is more important.

Comparison of the predicted performance of GRETA to the measured performance of Gammasphere demonstrates the potential improvements associated with the GRETA concept. In terms of the GRETA resolving power presented in [4], the peak performance of GRETA in the "with electron tracking" case (ε=0.22, P/T=0.61, RP=1.7 x 10^6) is seen to offer a ~600 fold gain over Gammasphere (where, from [4], RP=3 x 10^3).

7. Conclusion

Based on the algorithm presented in this paper, the GRETA concept would appear to offer (at M=25, E=1.332 MeV, Δr=2mm) at least a 2.5 fold gain in efficiency and a 1.2 fold gain in P/T over the performance of Gammasphere. This corresponds to a resolving power of 1.7 x 10^6, a ~600 fold gain over Gammasphere. It is hoped that these large potential gains will motivate further work in designing and developing the GRETA array.

Acknowledgments

The authors thank Matt Devlin (Washington Univ.) for providing us with details of his Gammasphere Monte Carlo simulation.

References

1. I.Y. Lee, Nucl. Phys A520, 641c (1990)
2. J. Simpson, Z Phys. A358, 139 (1997)
3. G.J. Schmid et al., IEEE Trans. Nucl. Sci., Vol. 44, No. 3, p.975, June, 1997
4. M.A. Deleplanque, et. al, "GRETA: Utilizing new concepts in γ-ray detection", in press, NIM A

5. R. Brun, F. Bruyant, M. Maire, et al., GEANT3 users' guide, DD/EE/84-1, CERN 1987
6. G.J. Schmid, A.O. Macchiavelli, et al., NIM A417, 95 (1998)
7. E. Aprile et al., NIM A327, 216 (1993)
8. P. Twin, B. Nyako, A. Nelson, et al., PRL 57, 811 (1986)
9. P.M. Jones, L. Wei, F.A. Beck, et al., NIM A362, 556 (1995)
10. A. von der Werth, F. Becker, J. Eberth, et al. NIM A357458 (1995)

Figure Captions

1. Results of "clustering only" algorithm (i.e. no tracking) for M=25, E_γ=1.332 MeV. Different position resolutions are shown.
2. Results of "clustering only" algorithm for M=25, E_γ=0.1 MeV. Single-hit photo-absorption events dominate at this energy.
3. Cluster modes for 400 M=25, E_γ=1.332 MeV events (10^4 γ rays in total). Infinitesimal position resolution (Δr=0mm) and a hypothetically perfect reconstruction are assumed. This plot indicates the maximum number of γ rays that can be recovered using each technique.
4. a) Histogram of the OFM for M=25, E_γ=1.332 MeV, Δr=1mm, showing the "good" and "bad" clusters.
   b) A histogram of the AFM for those events which fell outside an OFM<80 gate. By gating on AFM<100, we can now separate out most of the "add" cases.
5. Cluster modes for M=25, E_γ=1.332 MeV, Δr=0mm using the actual algorithm (10^4 γ rays total). Comparison with the hypothetical "best-case scenario" of Figure 3, one sees that the split mode is not well recovered.
6. Algorithm results for M=25 and E_γ=1.332 MeV as a function of α and Δr. The dashed line shows the measured performance of Gammasphere.
7. For M=25, α=10°, this plot shows the algorithm results vs. Δr and E_γ.
8. For E_γ=1.332 MeV, Δr=1mm, this plot shows the algorithm results vs. M and α.

9. Average event processing time for the algorithm as a function of Δr (for M=25, E_γ=1.332 MeV, α=10°).
10. Average event processing time for the algorithm as a function of M (for E_γ=1.332 MeV, α=10°, Δr=1mm).
11. Average event processing time as a function of α and E_γ (for M=25, Δr=1mm).
12. Average processing time for the various subroutines as a function of α (for E_γ=1.332 MeV, M=25, Δr=1mm).
13. For E_γ=1.332, M=25, Δr=1mm, the relative performance of locally-optimized vs. globally-optimized cuts is demonstrated.
14. The solid line shows the predicted response to the superdeformed band #1 in ^{152}Dy [8] with Δr=1mm. These results, using globally-optimized parameters, are compared to locally optimized results at 1.0 MeV (for M=25, Δr=1mm).
15. For 1.4 MeV (top) and 0.4 MeV (bottom) γ-rays, this graph shows the fraction of events which have had their 1st two points correctly identified in the tracking (assuming M=1 and at least 2 points in the cluster).
16. Polarization sensitivity (Q) as a function of Δr (assuming M=1, E_γ=400 keV). The dashed line represents the measured performance of the Gammasphere segmented Ge detectors [6].
17. Polarization sensitivity (Q) as a function of E_γ (assuming M=1, Δr=1mm). The dashed line represents the measured performance of the Gammasphere segmented Ge detectors [6].
18. Results using the realistic, 120 detector, geometry are shown by the diamond points (for M=25, E_γ=1.332 MeV, Δr=2mm). These diamond points include the effects of recoil e^- tracks. Also shown are the results for the Ge shell (circles), realistic geometry with no e^- tracking (squares), and the measured performance of Gammasphere (dashed line).

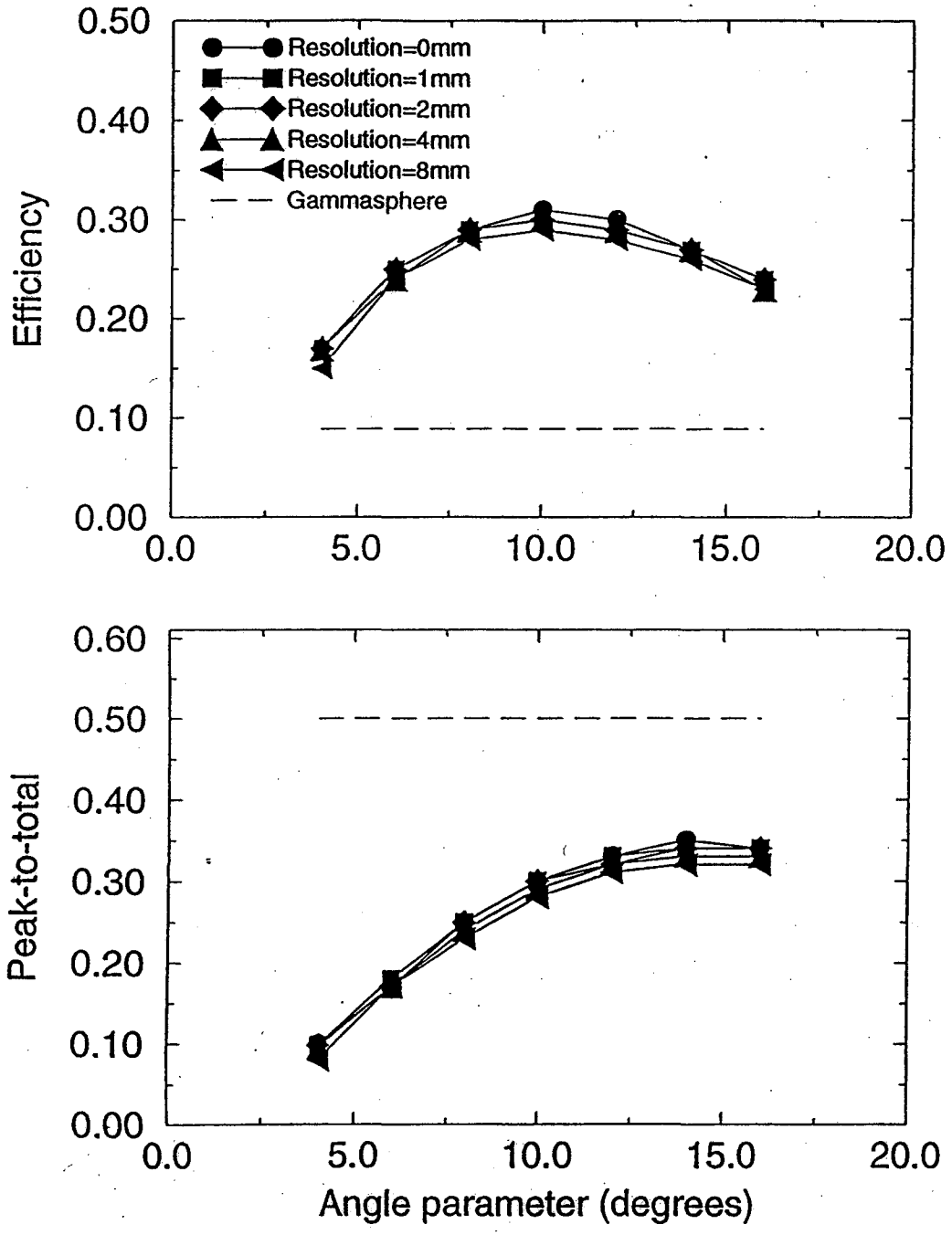
Efficiency
0.50
0.40
0.30
0.20
0.10
0.00
0.0
5.0
10.0
15.0
20.0
Resolution=0mm
Resolution=1mm
Resolution=2mm
Resolution=4mm
Resolution=8mm
Gammasphere
Peak-to-total
0.60
0.50
0.40
0.30
0.20
0.10
0.00
0.0
5.0
10.0
15.0
20.0
Angle parameter (degrees)

Fig.1

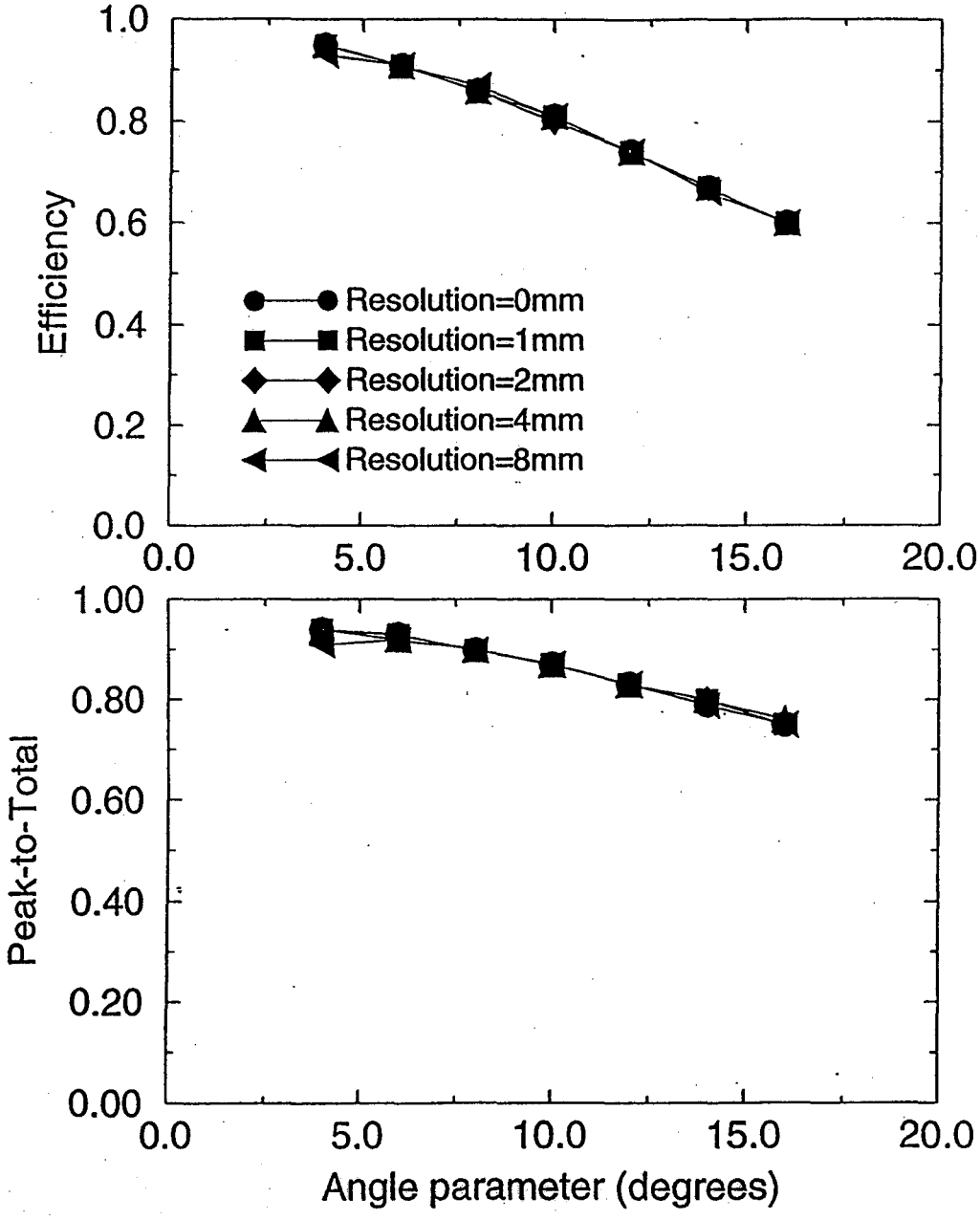
Efficiency
1.0
0.8
0.6
0.4
0.2
0.0
0.0
5.0
10.0
15.0
20.0
Resolution=0mm
Resolution=1mm
Resolution=2mm
Resolution=4mm
Resolution=8mm
Peak-to-Total
1.00
0.80
0.60
0.40
0.20
0.00
0.0
5.0
10.0
15.0
20.0
Angle parameter (degrees)

Fig.2

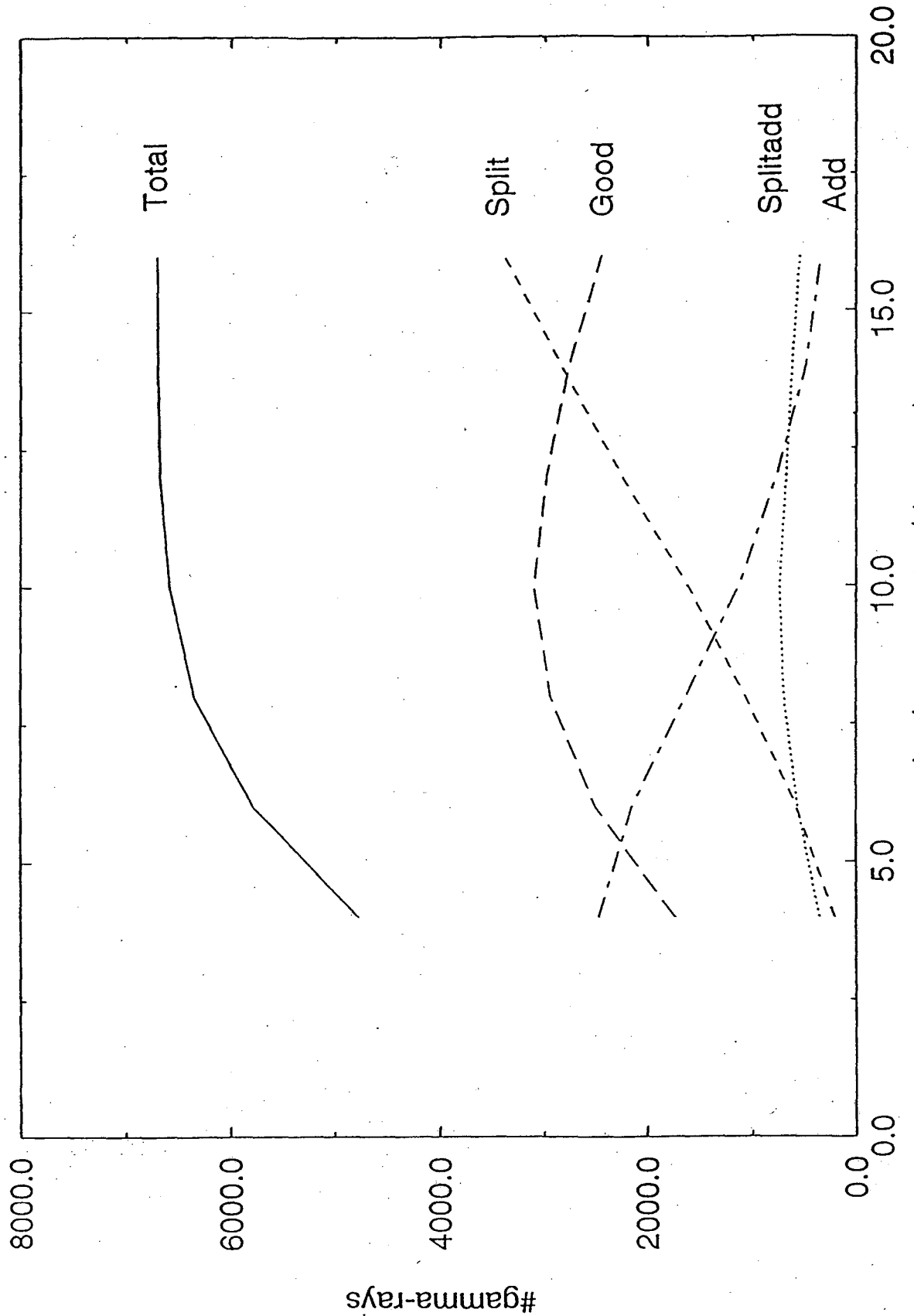
Total
Split
Good
Splitadd
Add
#gamma-rays
Angle parameter (degrees)
0.0
2000.0
4000.0
6000.0
8000.0
0.0
5.0
10.0
15.0
20.0

Fig.3

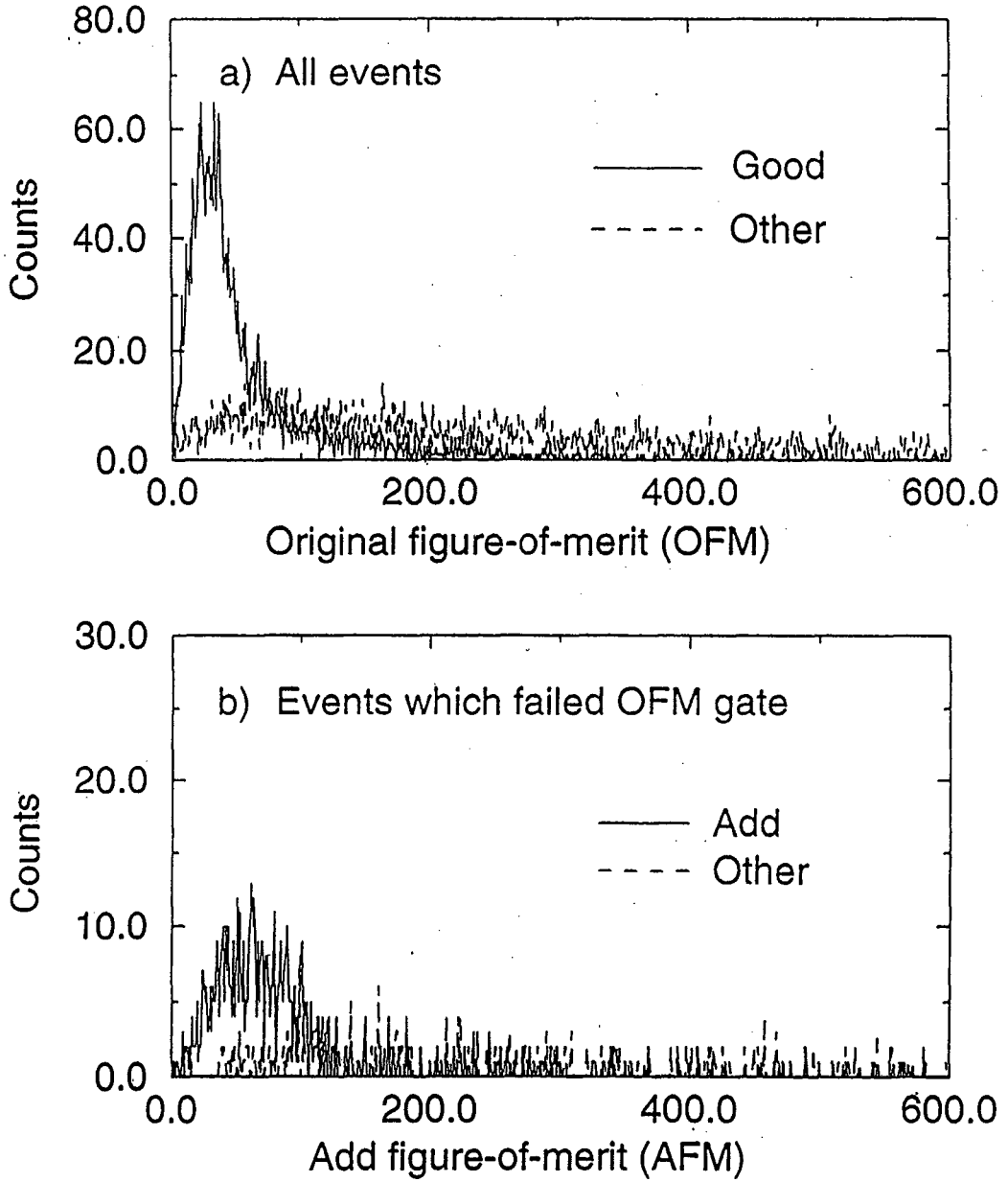
a) All events
Good
Other
Counts
80.0
60.0
40.0
20.0
0.0
0.0
200.0
400.0
600.0
Original figure-of-merit (OFM)
b) Events which failed OFM gate
Add
Other
Counts
30.0
20.0
10.0
0.0
0.0
200.0
400.0
600.0
Add figure-of-merit (AFM)

Fig.4

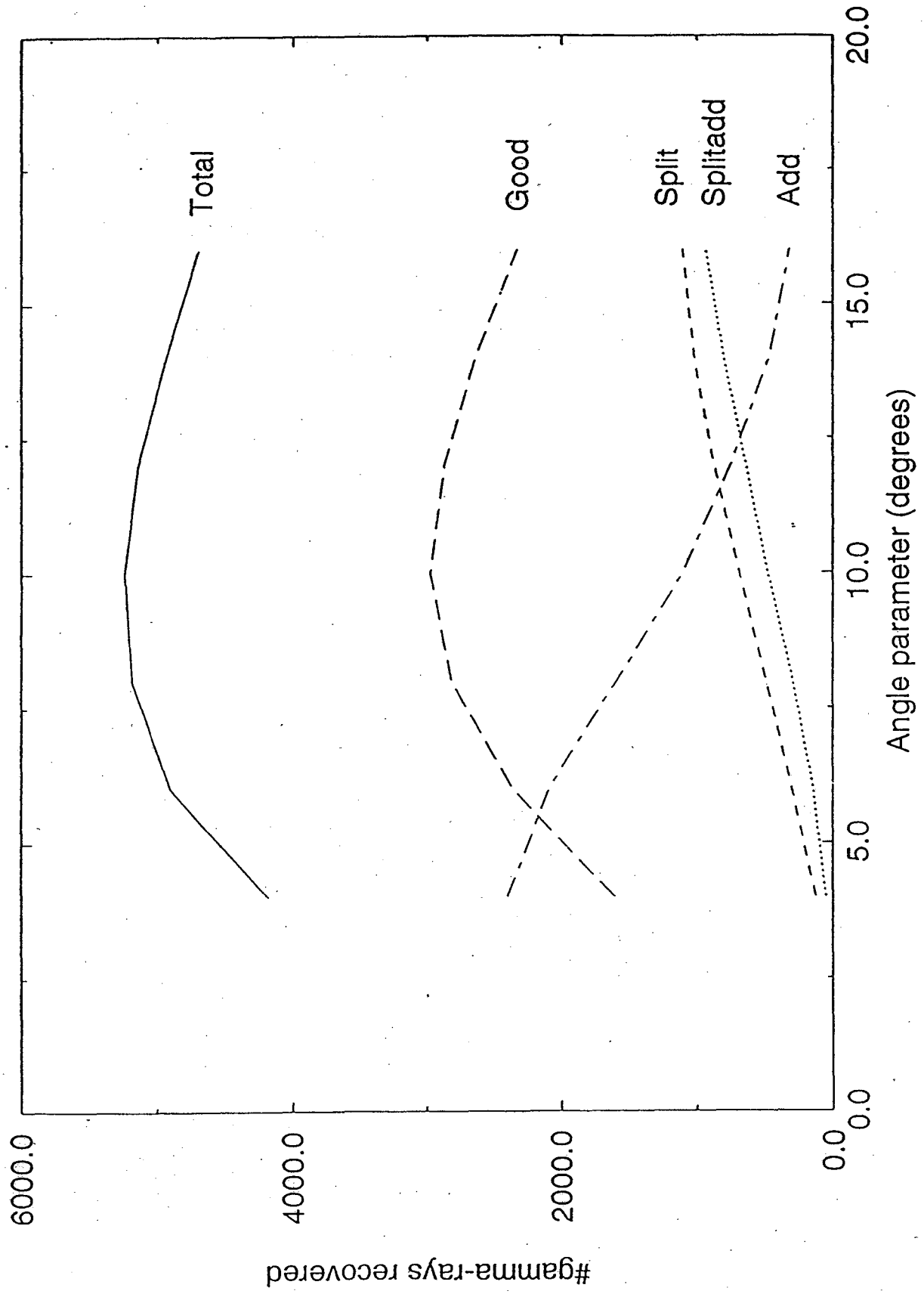
Total
Good
Split
Splitadd
Add
#gamma-rays recovered
Angle parameter (degrees)
0.0
2000.0
4000.0
6000.0
0.0
5.0
10.0
15.0
20.0

Fig.5

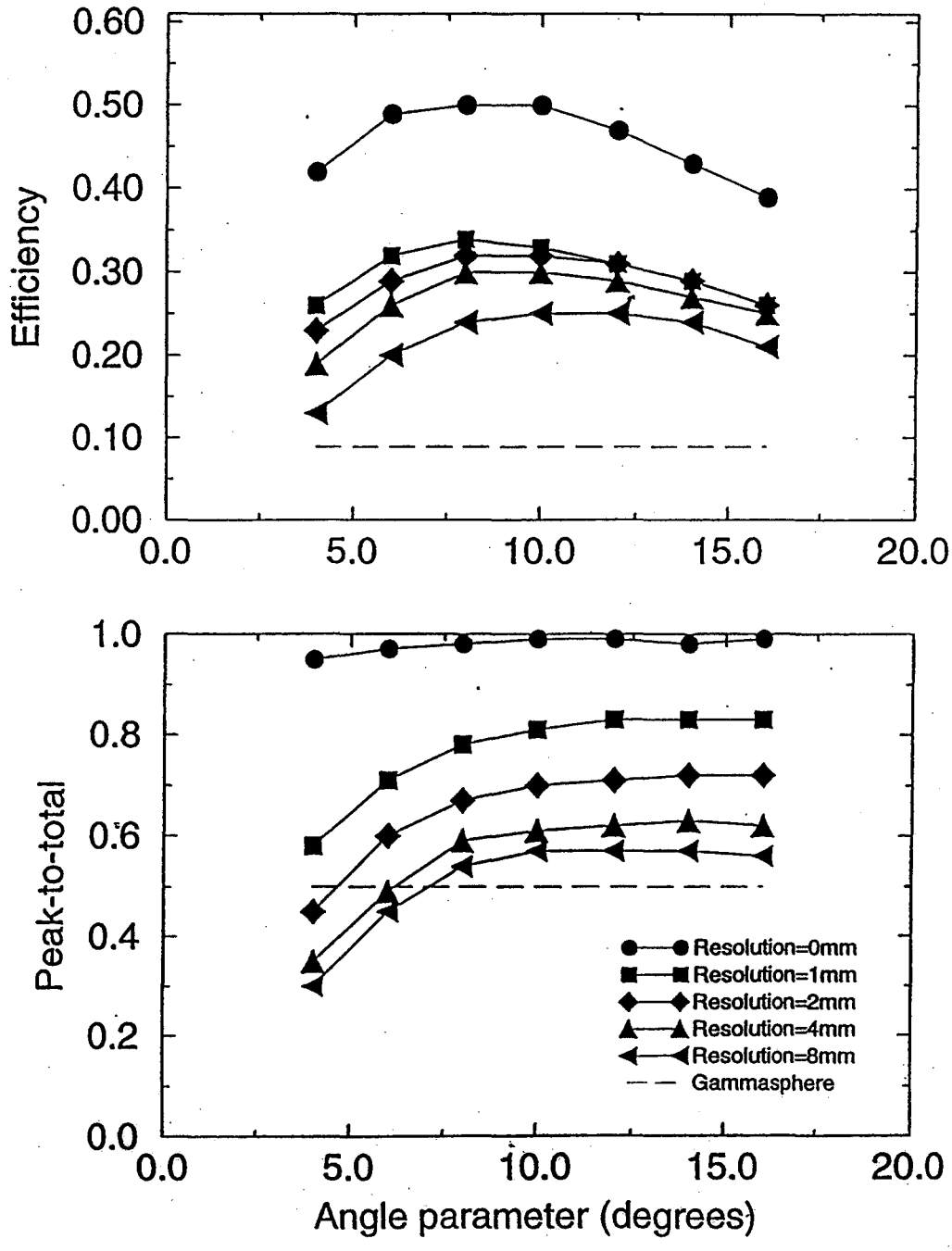
Efficiency
0.60
0.50
0.40
0.30
0.20
0.10
0.00
0.0
5.0
10.0
15.0
20.0
Peak-to-total
1.0
0.8
0.6
0.4
0.2
0.0
Resolution=0mm
Resolution=1mm
Resolution=2mm
Resolution=4mm
Resolution=8mm
Gammasphere
Angle parameter (degrees)

Fig.6

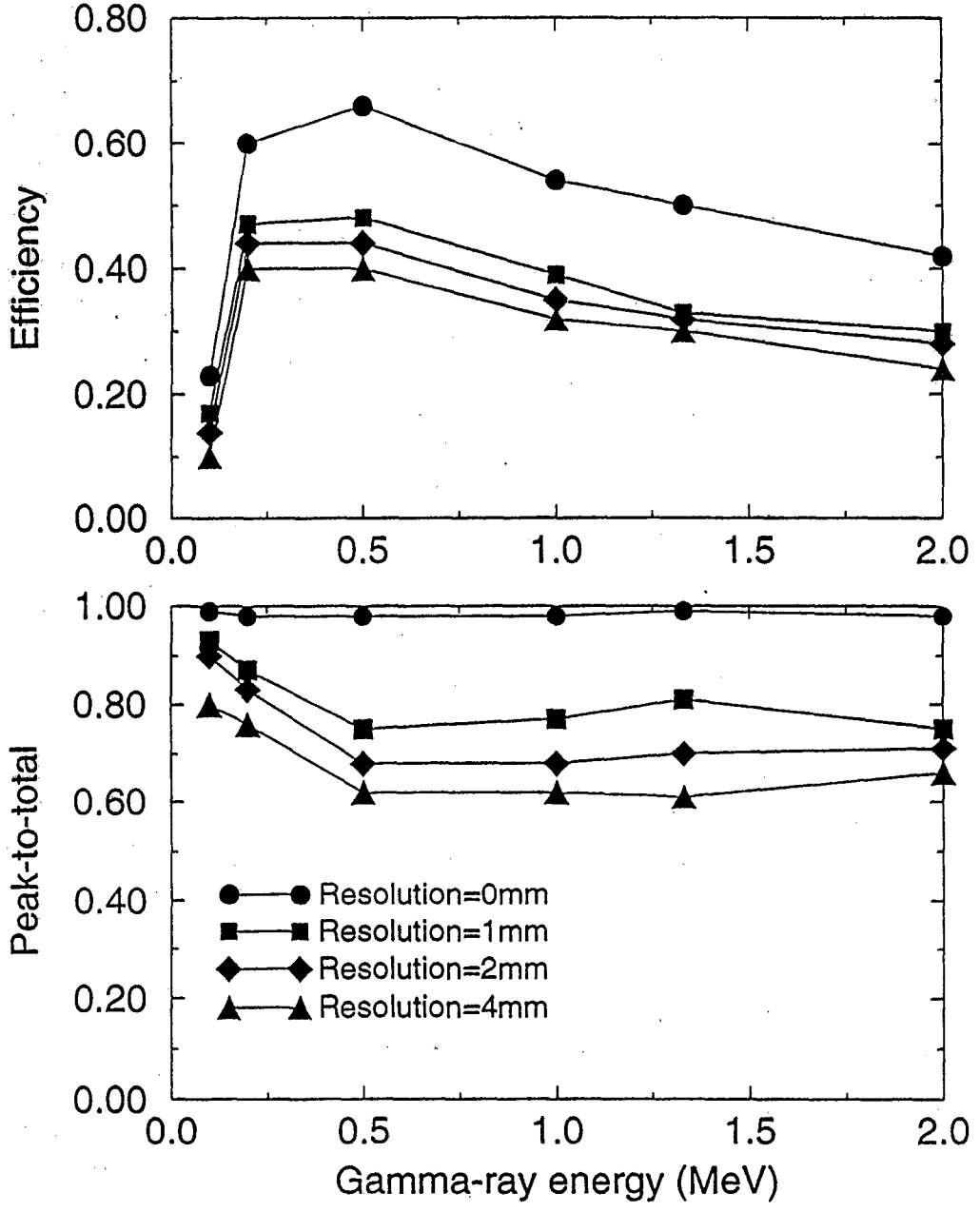
Efficiency
0.80
0.60
0.40
0.20
0.00
0.0
0.5
1.0
1.5
2.0
Peak-to-total
1.00
0.80
0.60
0.40
0.20
0.00
Resolution=0mm
Resolution=1mm
Resolution=2mm
Resolution=4mm
Gamma-ray energy (MeV)

Fig.7

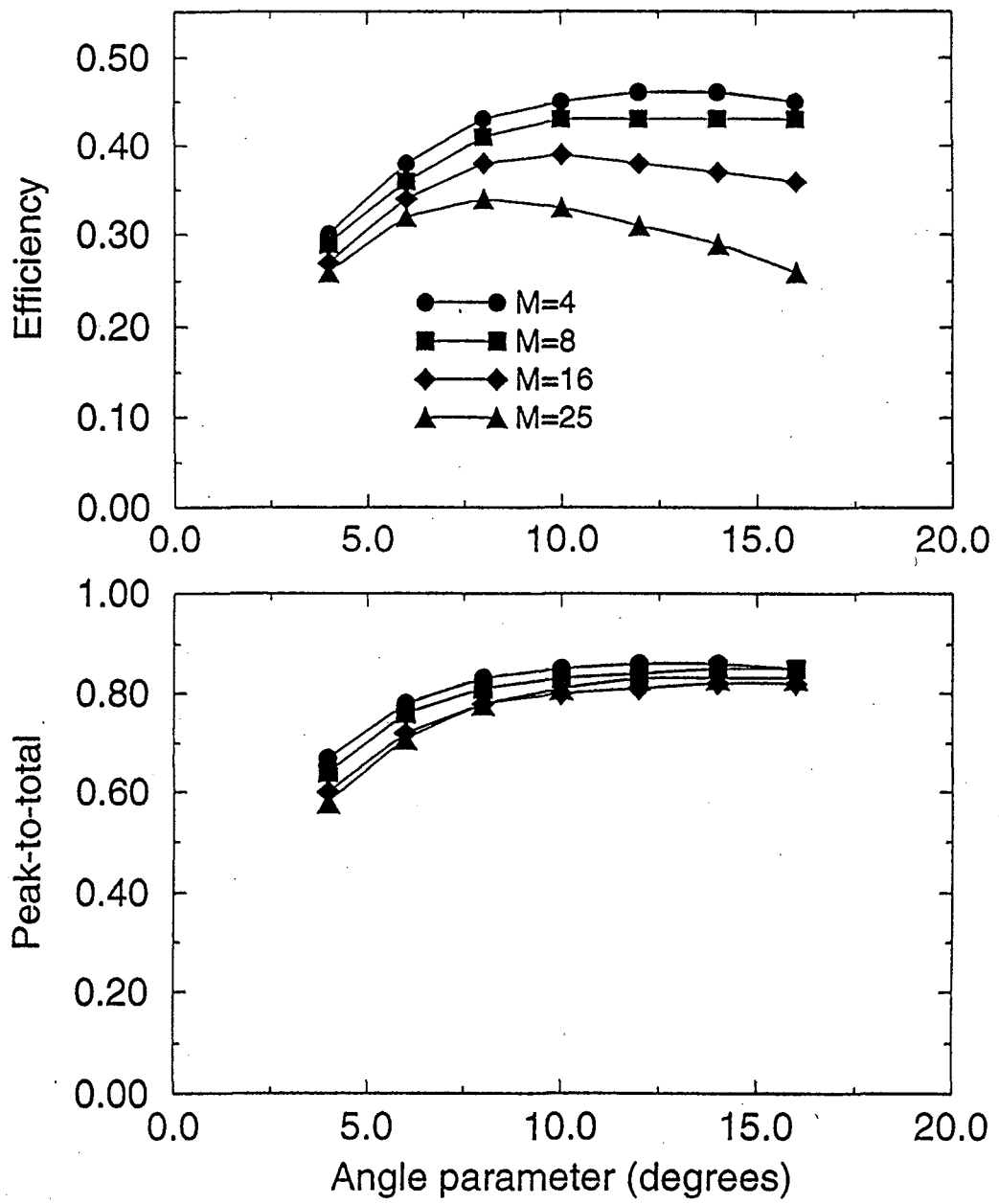
Efficiency
0.50
0.40
0.30
0.20
0.10
0.00
0.0
5.0
10.0
15.0
20.0
M=4
M=8
M=16
M=25
Peak-to-total
1.00
0.80
0.60
0.40
0.20
0.00
0.0
5.0
10.0
15.0
20.0
Angle parameter (degrees)

Fig.8

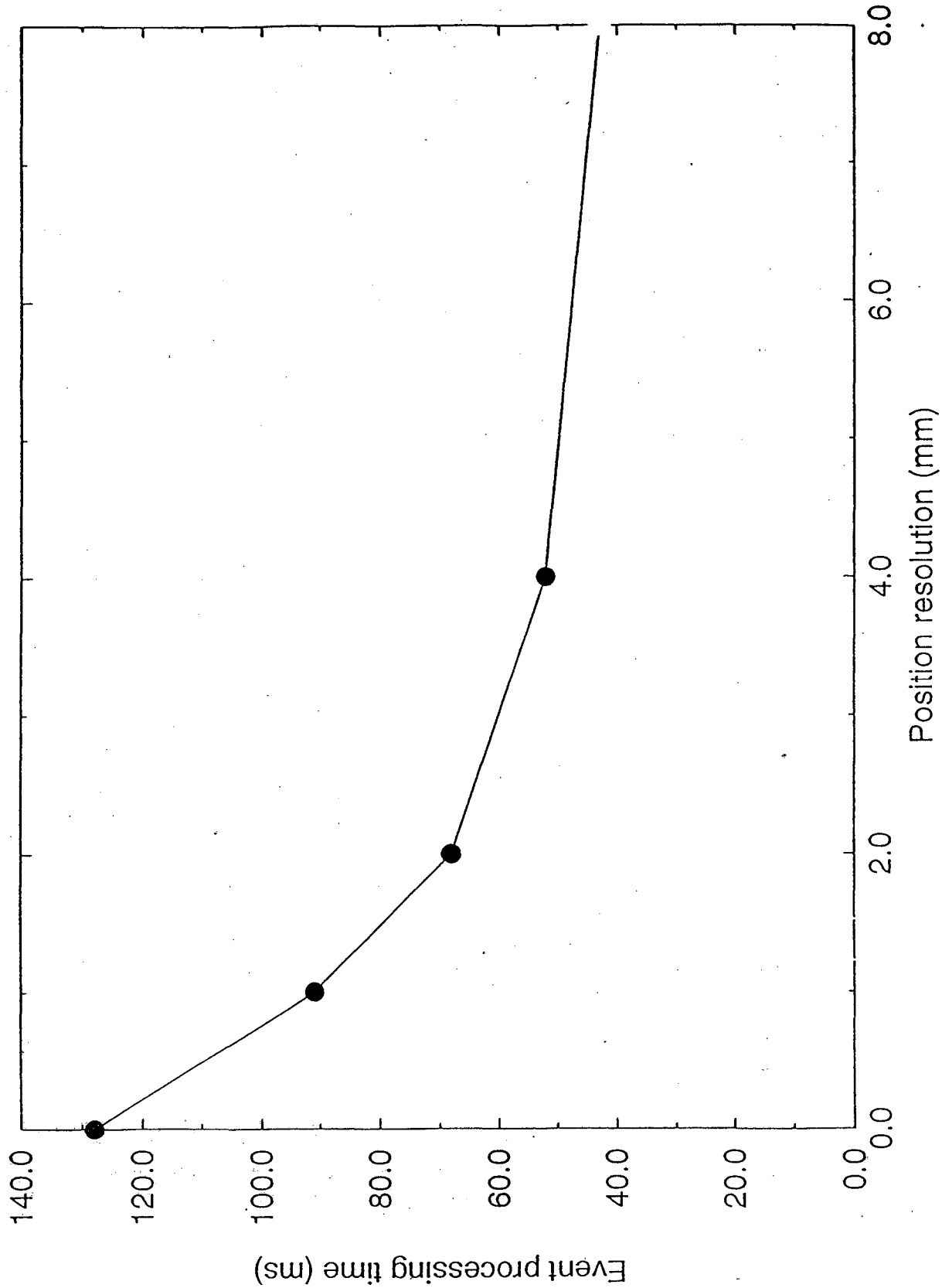
Event processing time (ms)
140.0
120.0
100.0
80.0
60.0
40.0
20.0
0.0
0.0
2.0
4.0
6.0
8.0
Position resolution (mm)

Fig.9

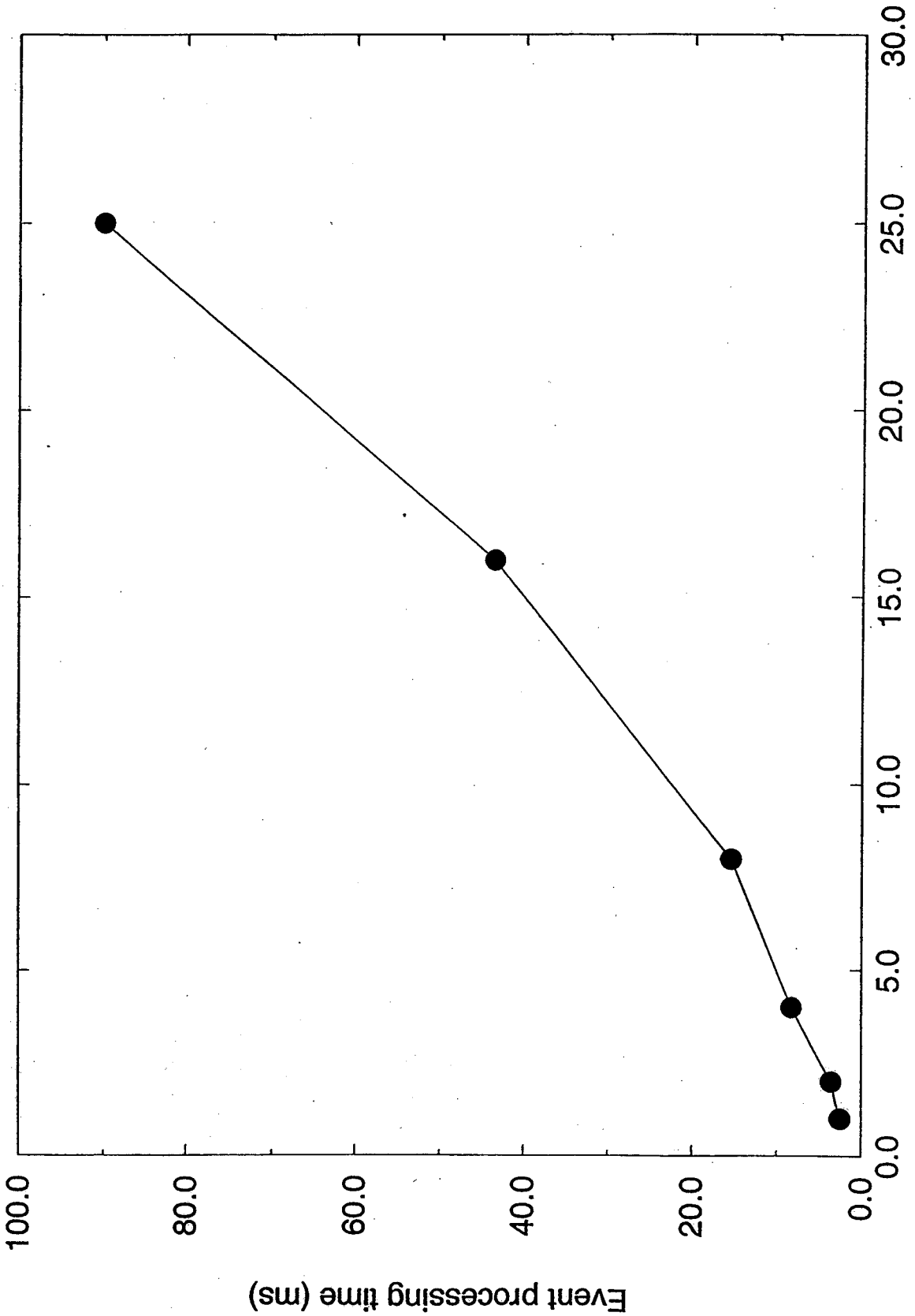
Event processing time (ms)
100.0
80.0
60.0
40.0
20.0
0.0
0.0
5.0
10.0
15.0
20.0
25.0
30.0
Gamma-ray multiplicity

Fig.10

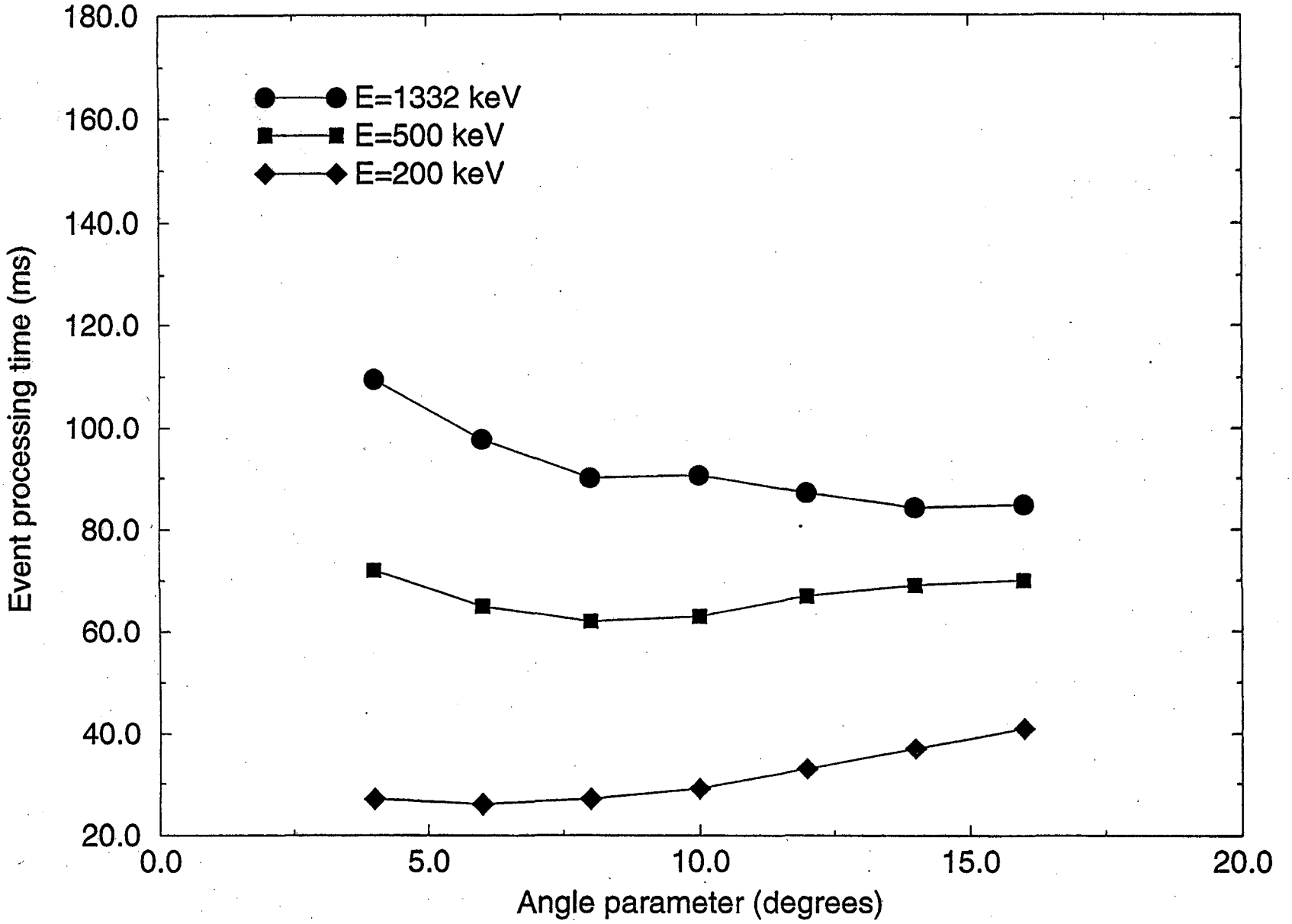
E=1332 keV
E=500 keV
E=200 keV
Event processing time (ms)
180.0
160.0
140.0
120.0
100.0
80.0
60.0
40.0
20.0
0.0
5.0
10.0
15.0
20.0
Angle parameter (degrees)

Fig.11

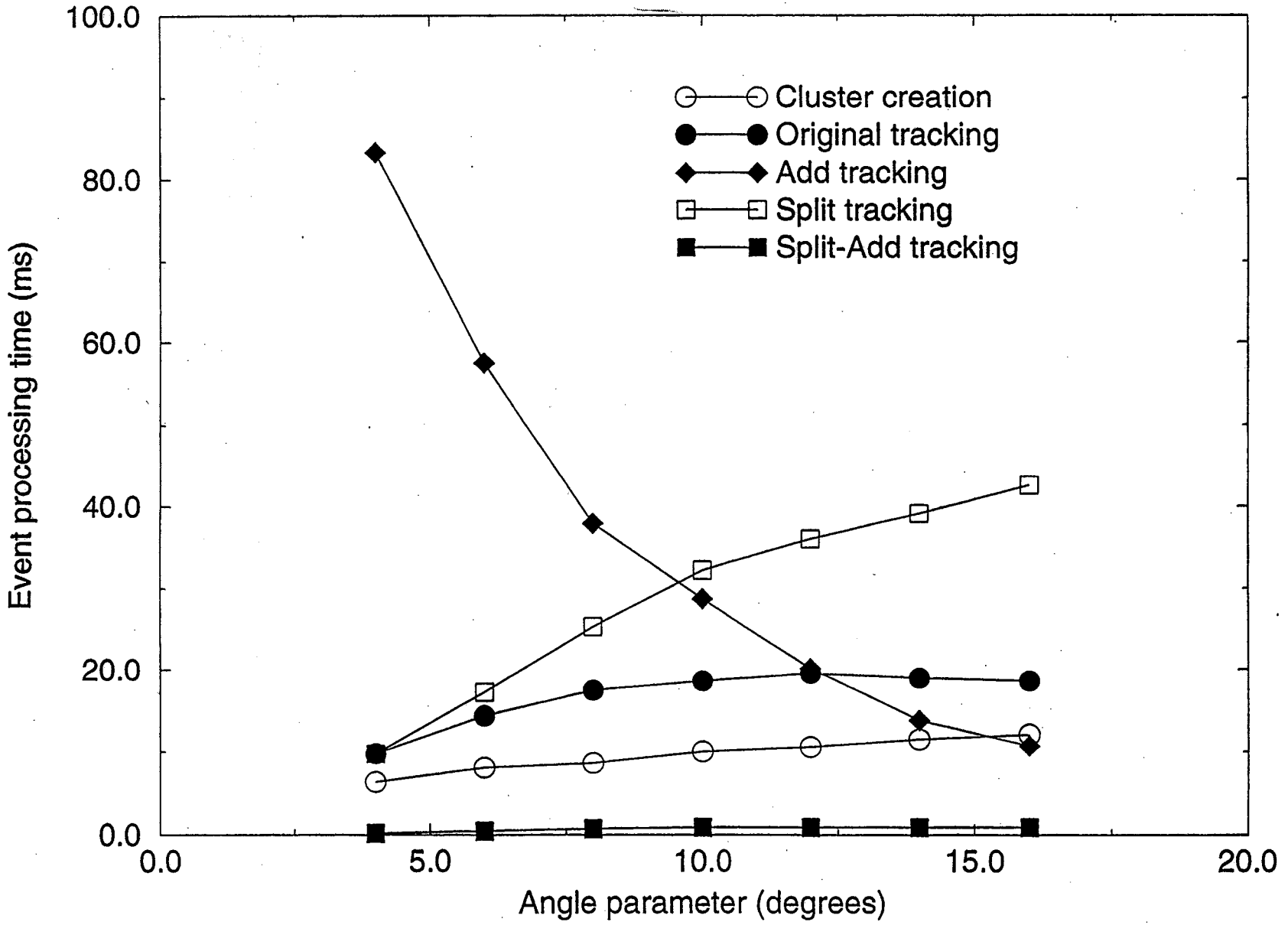
100.0
80.0
60.0
40.0
20.0
0.0
Event processing time (ms)
0.0
5.0
10.0
15.0
20.0
Angle parameter (degrees)
Cluster creation
Original tracking
Add tracking
Split tracking
Split-Add tracking

Fig.12

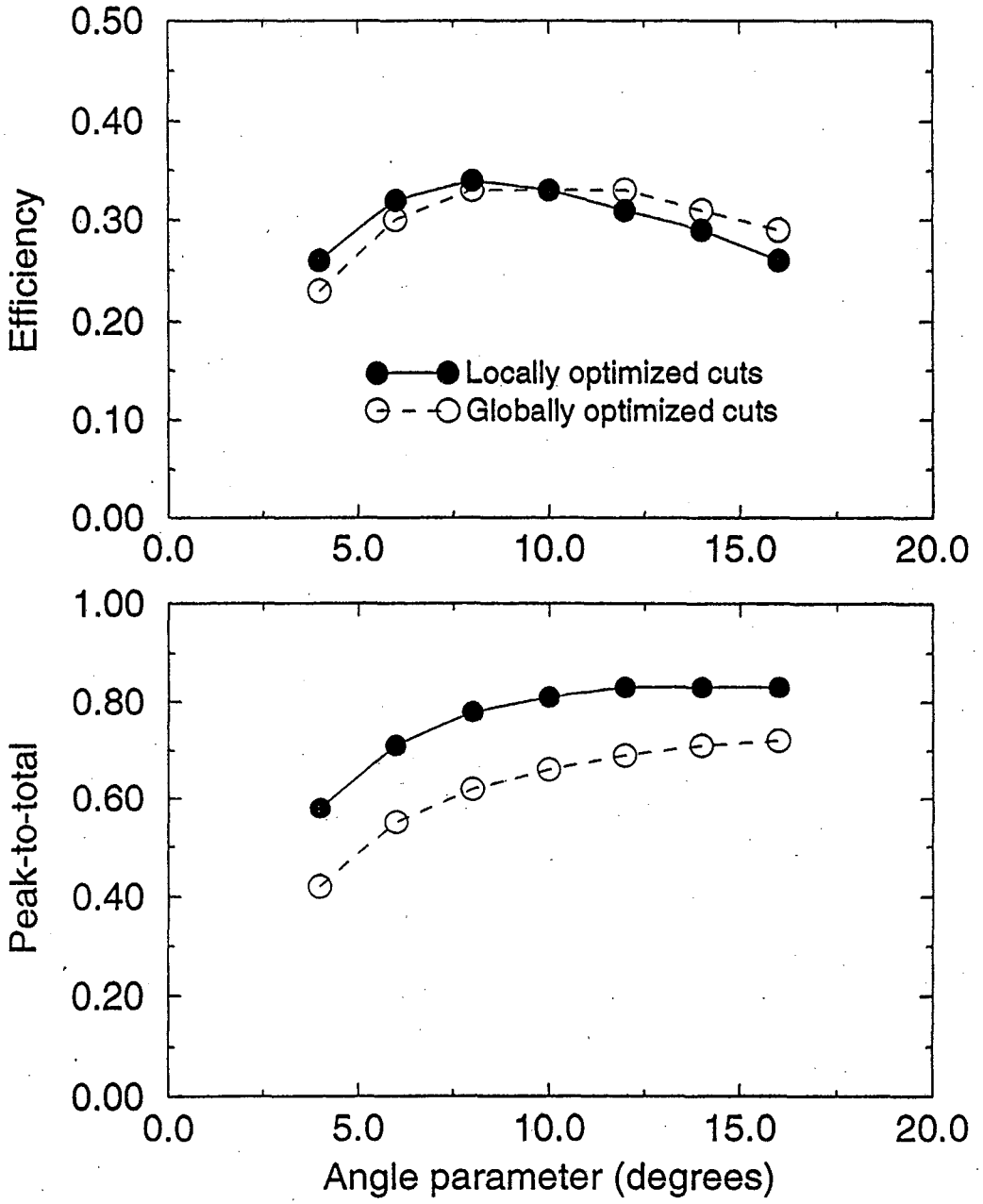
0.50
0.40
0.30
0.20
0.10
0.00
Efficiency
Locally optimized cuts
Globally optimized cuts
0.0
5.0
10.0
15.0
20.0
1.00
0.80
0.60
0.40
0.20
0.00
Peak-to-total
0.0
5.0
10.0
15.0
20.0
Angle parameter (degrees)

Fig.13

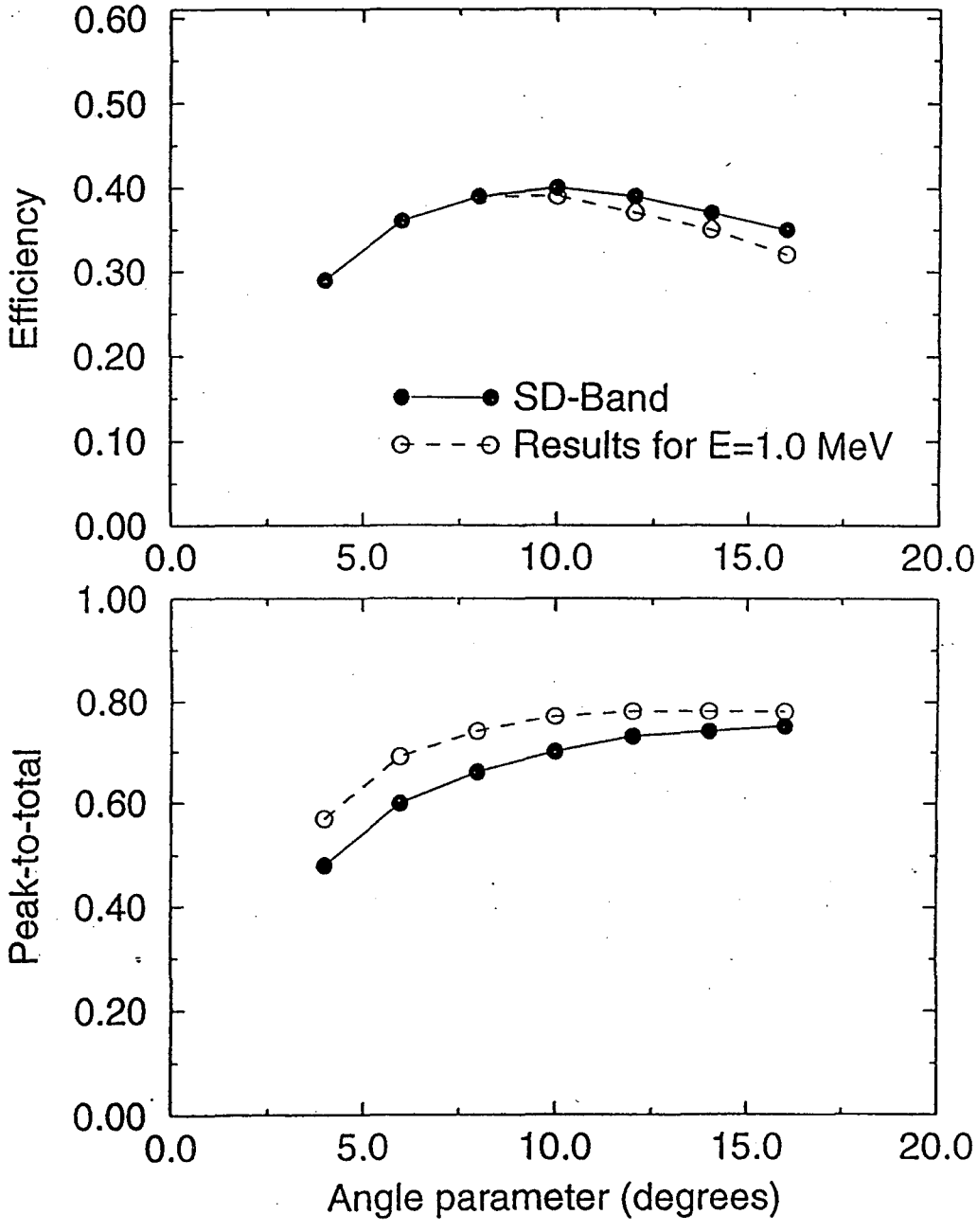
Efficiency
0.60
0.50
0.40
0.30
0.20
0.10
0.00
SD-Band
Results for E=1.0 MeV
0.0
5.0
10.0
15.0
20.0
Peak-to-total
1.00
0.80
0.60
0.40
0.20
0.00
0.0
5.0
10.0
15.0
20.0
Angle parameter (degrees)

Fig.14

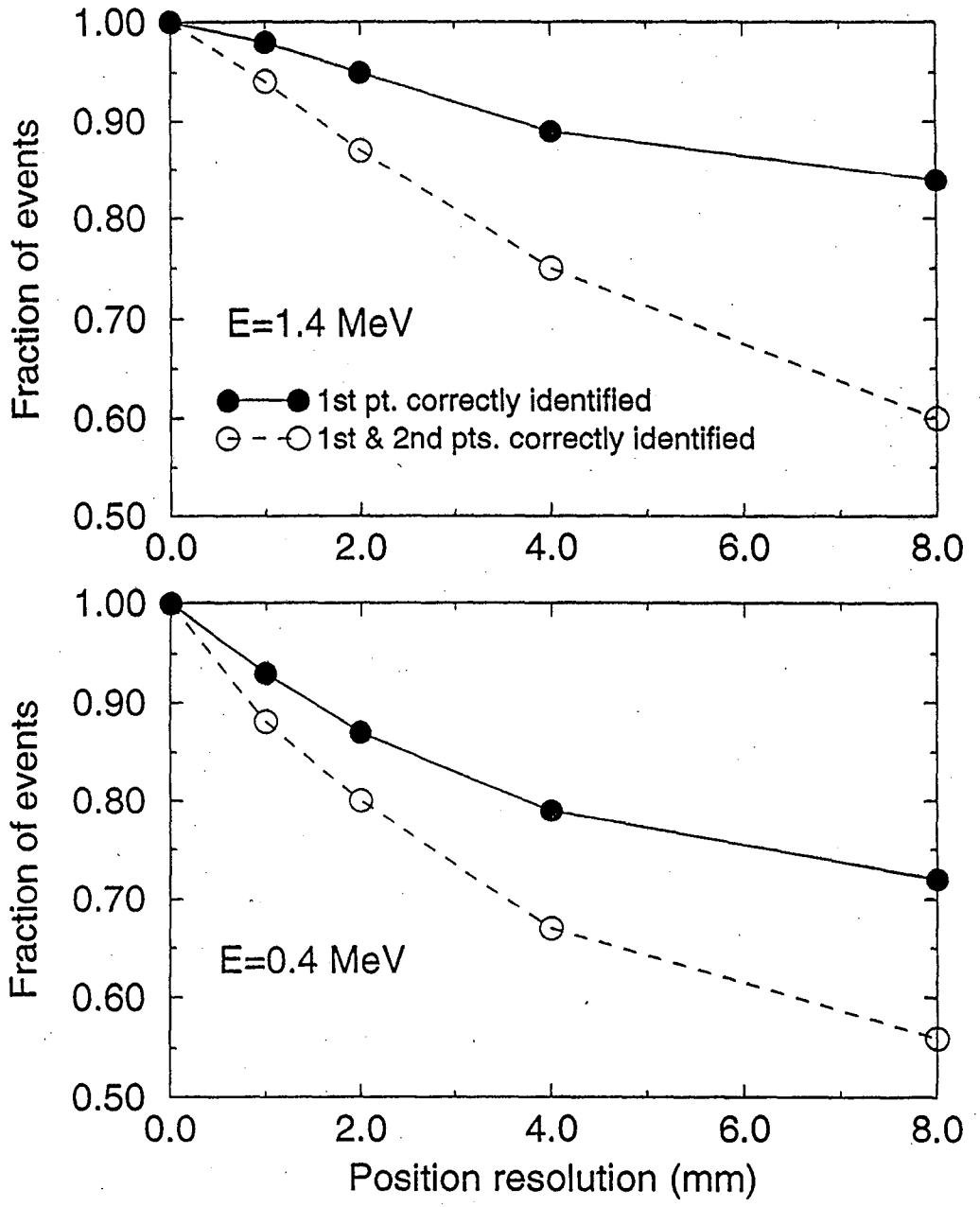
1.00
0.90
0.80
0.70
0.60
0.50
Fraction of events
E=1.4 MeV
1st pt. correctly identified
1st & 2nd pts. correctly identified
0.0
2.0
4.0
6.0
8.0
E=0.4 MeV
Position resolution (mm)

Fig.15

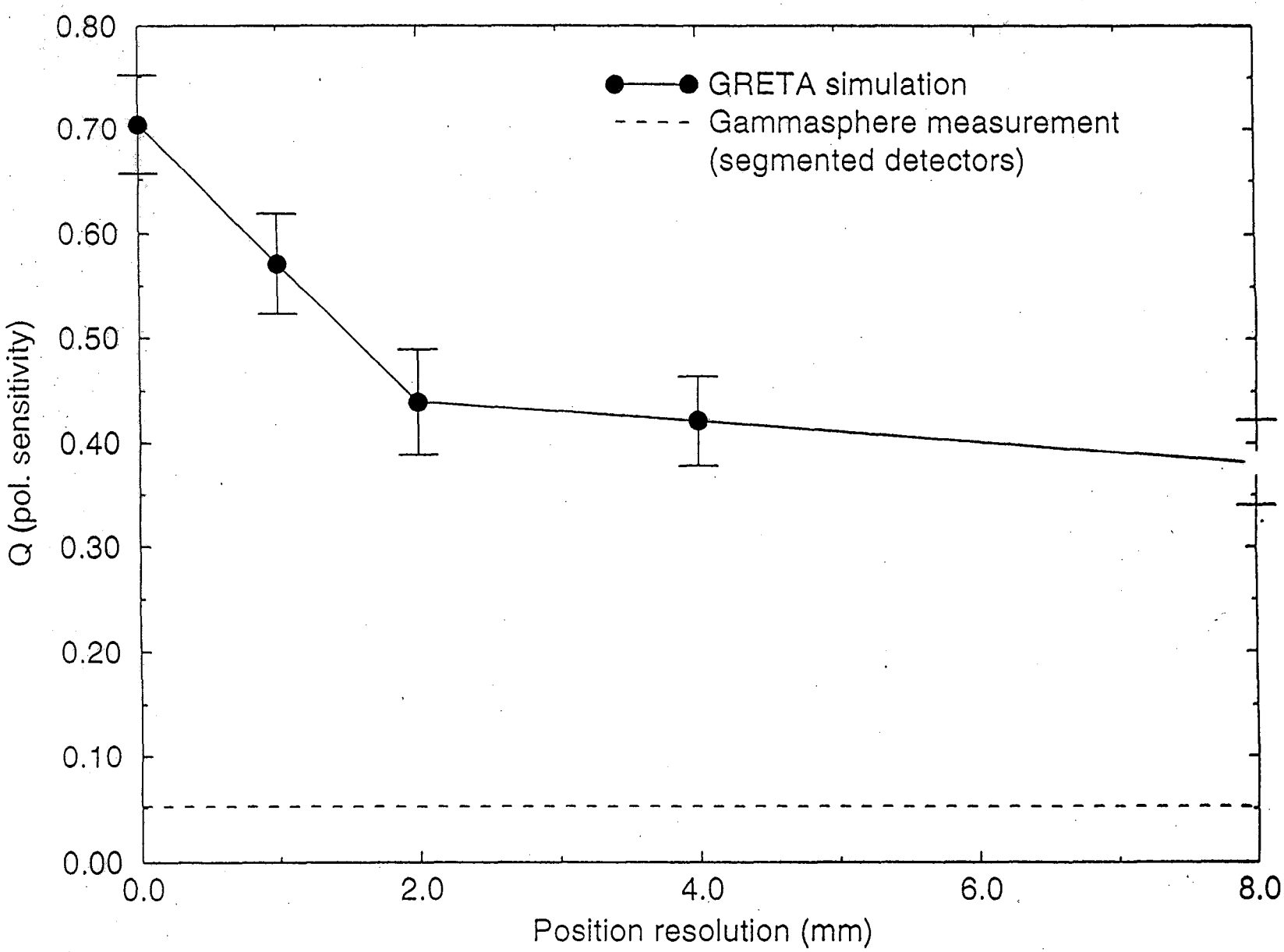
0.80
0.70
0.60
0.50
0.40
0.30
0.20
0.10
0.00
Q (pol. sensitivity)
0.0
2.0
4.0
6.0
8.0
Position resolution (mm)
GRETA simulation
Gammasphere measurement
(segmented detectors)

Fig.16

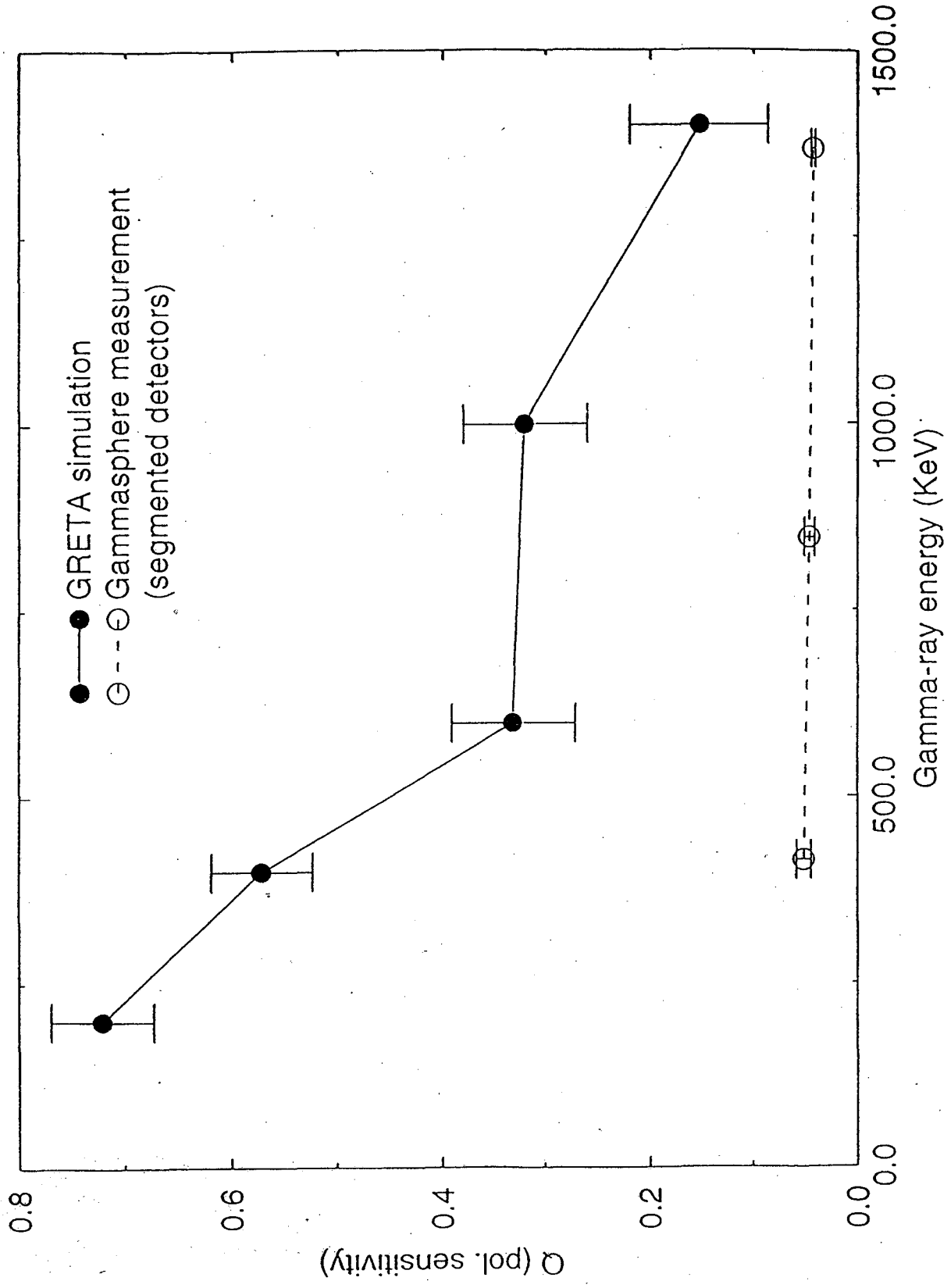
GRETA simulation
Gammasphere measurement
(segmented detectors)
Q (pol. sensitivity)
Gamma-ray energy (KeV)
0.0
0.2
0.4
0.6
0.8
500.0
1000.0
1500.0

Fig.17

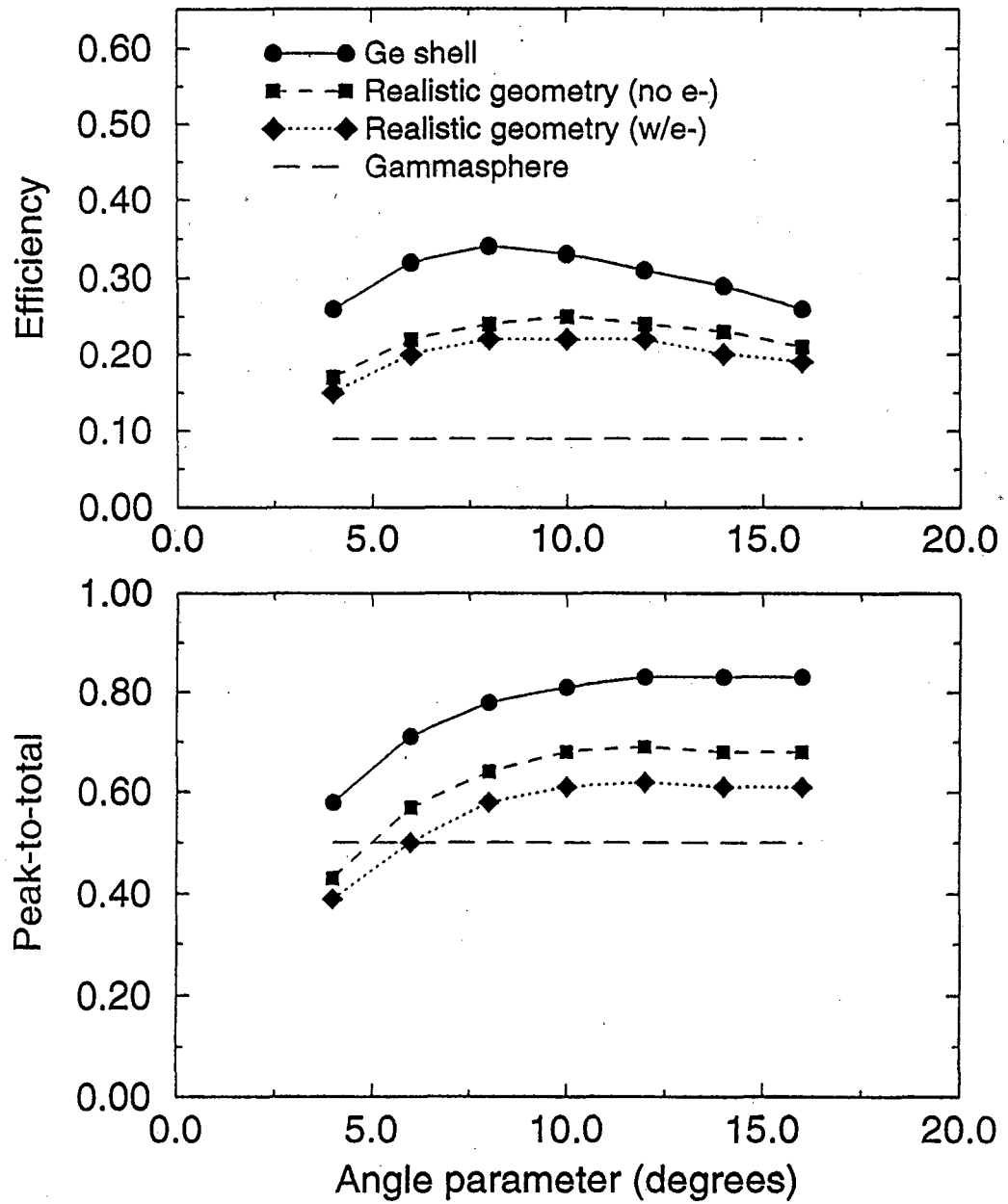
Ge shell
Realistic geometry (no e-)
Realistic geometry (w/e-)
Gammasphere
Efficiency
0.60
0.50
0.40
0.30
0.20
0.10
0.00
0.0
5.0
10.0
15.0
20.0
Peak-to-total
1.00
0.80
0.60
0.40
0.20
0.00
Angle parameter (degrees)

Fig.18

Ernest Orlando Lawrence Berkeley National Laboratory
One Cyclotron Road | Berkeley, California 94720

Prepared for the U.S. Department of Energy under Contract No. DE-AC03-76SF00098